ERDC/CRREL TR-20-3

US Army Corps of Engineers®
Engineer Research and Development Center

ERDC
ENGINEER RESEARCH & DEVELOPMENT CENTER

*Environmental Security Technology Certification Program (ESTCP)*
*Environmental Restoration Program*

# Sieve Stack and Laser Diffraction Particle Size Analysis of IMX-104 Low-Order Detonation Particles

Matthew F. Bigl, Samuel A. Beal, Michael R. Walsh,
Charles A. Ramsey, and Katrina M. Burch

February 2020

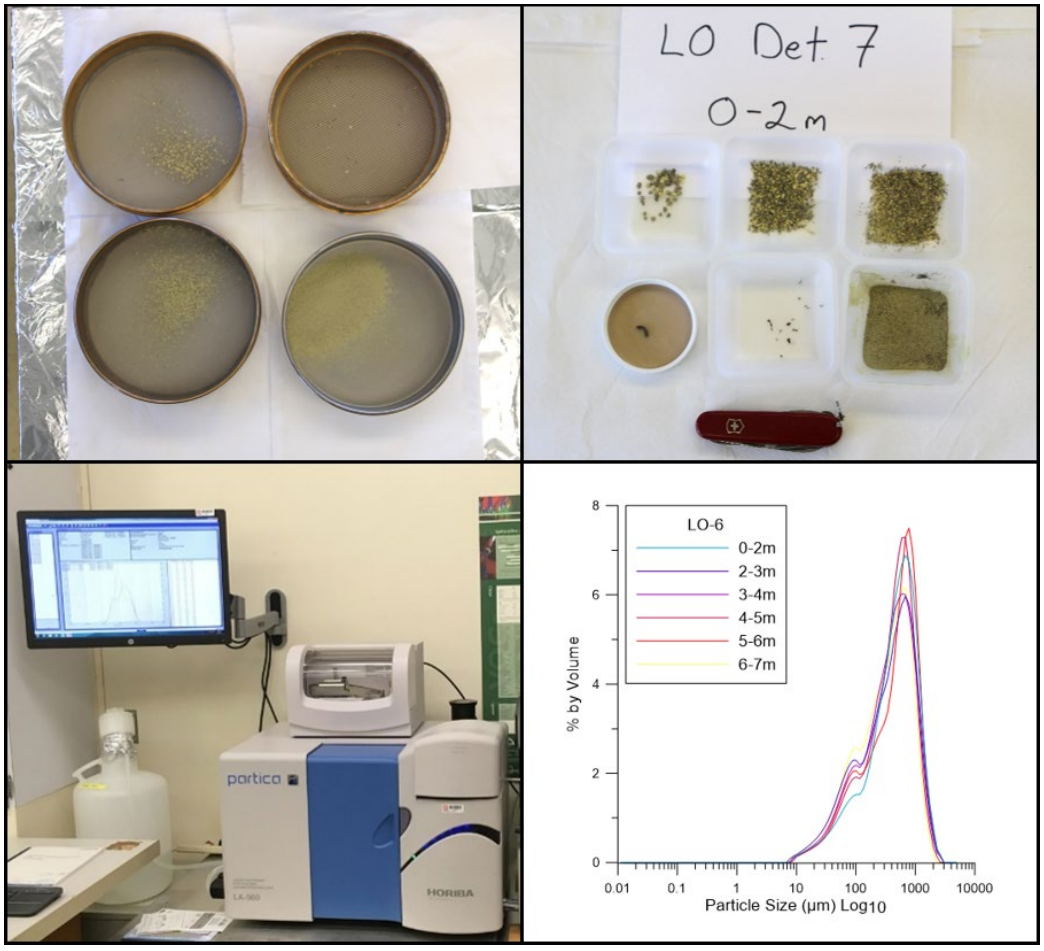


Cold Regions Research and Engineering Laboratory

Approved for public release; distribution is unlimited.

**The U.S. Army Engineer Research and Development Center (ERDC)** solves the nation's toughest engineering and environmental challenges. ERDC develops innovative solutions in civil and military engineering, geospatial sciences, water resources, and environmental sciences for the Army, the Department of Defense, civilian agencies, and our nation's public good. Find out more at www.erdc.usace.army.mil.

To search for other technical reports published by ERDC, visit the ERDC online library at http://acwc.sdp.sirsi.net/client/default.

Environmental Security Technology
Certification Program (ESTCP)
Environmental Restoration Program

ERDC/CRREL TR-20-3
February 2020

# Sieve Stack and Laser Diffraction Particle Size Analysis of IMX-104 Low-Order Detonation Particles

Matthew F. Bigl, Samuel A. Beal, Michael R. Walsh, and Katrina M. Burch

*U.S. Army Engineer Research and Development Center (ERDC)*
*Cold Regions Research and Engineering Laboratory (CRREL)*
*72 Lyme Road*
*Hanover, NH 03755-1290*

Charles A. Ramsey

*Envirostat, Inc.*
*PO Box 339*
*Vail, AZ 85641*

Final Report

Approved for public release; distribution is unlimited.

Prepared for Environmental Security Technology Certification Program
Environmental Restoration Program Area
4800 Mark Center Drive, Suite 16F16
Alexandria, VA 22350-3605

Under MIPR W74RDV80715663 and W74RDV90156248

# Abstract

When an artillery round undergoes a low-order detonation during live-fire training or an unexploded ordnance clearance operation, up to 25% of the round's energetic contents are scattered over a small, localized area, sometimes less than 100 $m^2$. Training-range fate and transport models require an accurate representation of the particle-size characteristics of the material left behind from low-order detonations.

This study investigated using laser diffraction particle size analysis to characterize 26 samples collected from four low-order command-detonated 81 mm mortar bodies filled with IMX-104. The refractive index of IMX-104 was estimated using an iterative recalculation technique on a Horiba LA-960 that yielded 1.845 0.01*i*. Of the 25 triplicate analyses conducted using this value, 12 passed the USP <429> measurement standard with 9 of the remaining samples found to have had a reduction in particle size during analysis that caused artificially high coefficient of variance values. The cumulative percent of particle sizes determined by laser diffraction and sieve stack differed by 0%–21.9% (median = 0.2%–7.2%). In addition, the higher resolution results of the laser diffraction particle size analysis, especially for particles smaller than 0.5 mm, make it the preferred method of analysis.

**DISCLAIMER:** The contents of this report are not to be used for advertising, publication, or promotional purposes. Citation of trade names does not constitute an official endorsement or approval of the use of such commercial products. All product names and trademarks cited are the property of their respective owners. The findings of this report are not to be construed as an official Department of the Army position unless so designated by other authorized documents.

**DESTROY THIS REPORT WHEN NO LONGER NEEDED. DO NOT RETURN IT TO THE ORIGINATOR.**

# Contents

**Abstract** ..... ii

**Figures and Tables** ..... iv

**Preface** ..... vi

**Acronyms and Abbreviations** ..... vii

**1 Introduction** ..... 1

1.1 Background ..... 1
1.2 Objectives ..... 3
1.3 Approach ..... 3

**2 Methods** ..... 4

2.1 March 2015 command-detonation testing and sampling ..... 4
2.2 Particle isolation ..... 6
2.3 Sieve stack analysis ..... 8
2.4 Estimation of refractive index ..... 9
2.5 Laser diffraction particle size analysis ..... 10

**3 Results and Discussion** ..... 12

3.1 Sieve stack analysis ..... 12
*3.1.1 Low-order detonations* ..... *12*
*3.1.2 Partial detonations* ..... *13*
3.2 Estimation of refractive index using the Horiba LA-960 ..... 14
3.3 Laser diffraction particle size analysis ..... 23
3.4 Sieve stack and LD-PSA comparison ..... 25

**4 Conclusions** ..... 28

**References** ..... 30

**Appendix A: PSDs That Did Not Pass CV Test** ..... 33

**Appendix B: PSDs That Passes the Triplicate Analyses CV Standard for D10, D50, and D90** ..... 37

**Appendix C: LD-PSA and Sieve Stack Comparison Plots for All Samples** ..... 40

**Appendix D: PSD Plots for All Samples Sieved <2 mm** ..... 45

**Appendix E: Cumulative Percent Data** ..... 50

**Report Documentation Page**

# Figures and Tables

## Figures


1 An 81 mm IMX-104 mortar body with CFS and C4 booster load ..... 4
2 Marking 1 m annuli around the detonation point. Rings were marked in alternating colors ..... 5
3 VirTis Freezemobile 12XL freeze-dryer loaded with 2015 particle samples ..... 6
4 Top-view of 8 oz jars filled with a split sample and topped with filters and ring caps ..... 7
5 Detail view of VirTis Freezemobile 12XL with 2015 samples ..... 8
6 Sieve stack setup in the fume hood and the resulting particle-size fractions and debris ..... 8
7 Parameters for RI 1 and imaginary components ranging from 0.95 to 0.99 ..... 16
8 R parameters for RI 2 and imaginary components ranging from 0 to 0.6 (0.7 is not shown because it returned a value of 0) ..... 16
9 R parameters for RI of 1.5–2.5 with a fixed imaginary component of 0.01 ..... 17
10 Detail view of the lowest R parameter data for RI of 1.5–2.5 with a fixed imaginary component of 0.01 ..... 17
11 Detail view of the lowest R parameter data for RI of 1.800–1.905 with a fixed imaginary component of 0.01 ..... 18
12 PSD plots of LO particle samples with the highest change in CV for D10 and D50 ..... 20
13 Bar plot of LO-2 samples that did not pass the CV standard with a reduction in D10, D50, D90, and mean particle-size values. The full table of values is in Appendix A ..... 21
14 Bar plot of LO-2 samples that did not pass the CV standard with varying change in D10, D50, D90, and mean particle-size values. The full table of values is in Appendix A ..... 21
15 Bar plot of LO-6 samples that did not pass the CV standard with decreasing D10, D50, D90, and mean particle-size values. The full table of values is in Appendix A ..... 22
16 Bar Plot of LO-7 samples that did not pass the CV standard with varying change in D10, D50, D90, and mean particle size. The full table of values is in Appendix A ..... 22
17 PSDs for LO-2, -3, -6, and -7 as measured by the Horiba LA-960 ..... 24
18 Step graphs of the cumulative percent by mass of sieve stack data overlain by cumulative percent by volume curves from LD-PSA from the same samples ..... 26
A-1 Full set of PSD plots of LO particle samples that did not pass the CV test ..... 33
A-2 Summary of D10, D50, D90, and mean particle size for all samples that did not pass the CV standard ..... 36
B-1 Full set of PSD plots of LO particle samples that passed the CV test ..... 37
C-1 Cumulative percent by mass of sieve stack data overlain by cumulative percent by volume curves from LD-PSA for all samples analyzed ..... 40

D-1 Particle size distributions for Run 1 of all samples analyzed ..... 45

## Tables

1 Detonation characterization descriptors based on conventional munitions ..... 2
2 Low-order detonation tests from March 2015 with estimated detonation type. Adapted from M. R. Walsh et al. (2017) ..... 5
3 Detonation results from low-order detonation tests, March 2015. Adapted from M. R. Walsh et al. (2017) ..... 12
4 Distribution statistics for LO-3 and -7 based on sieve size ..... 13
5 Distribution statistics for LO-3 and -7 based on annuli distance ..... 13
6 Distribution statistics for LO-2 and -6 based on sieve size ..... 14
7 Distribution statistics for LO-2 and -6 based on annuli distance ..... 14
8 Summary of R parameter data for step one of the RI estimation for LO-2 particle analysis ..... 15
9 Summary of CV values calculated for triplicate runs of LO-2, -3, -6, and -7 ..... 19
E-1 Cumulative percent data from sieve stack and LD-PSA analysis of the same sample. LD-PSA data has been down selected by sieve bin size for direct comparison ..... 50

# Preface

This research was sponsored by the Environmental Security Technology Certification Program (ESTCP) under Environmental Restoration program project number ER18-5105, "Determination of Residual Low-Order Detonation Particle Characteristics." Funding was provided by MIPR W74RDV80715663 and W74RDV90156248. Dr. Herb Nelson was Executive Director for ESTCP, and Dr. Andrea Leeson was Deputy Director and Project Monitor.

This report was prepared by the Engineering Resources Branch (ERB), the Biogeochemical Sciences Branch (BSB), and the Signature Physics Branch (SPB) of the Research and Engineering Division, U.S. Army Engineer Research and Development Center, Cold Regions Research and Engineering Laboratory (ERDC-CRREL). Researchers from ERDC-CRREL collaborated with Envirostat, Inc, of Vail, Arizona. At the time of publication, Mr. Jared Oren was Chief, ERB; Dr. Justin Berman was Chief, BSB; Dr. Andrew Niccolai was Chief, SPB; and Mr. J. D. Horne was Division Chief. The Deputy Director of ERDC-CRREL was Mr. David B. Ringelberg, and the Director was Dr. Joseph L. Corriveau.

The authors acknowledge Mr. Brandon Booker of ERDC-CRREL for experimentation support. The authors would also like to thank all members of Strategic Environmental Research and Development Program (SERDP) ER-2219 for collecting the samples and providing data used for this study. Mr. Brian P. Hubbard provided manuscript review on behalf of Joint Program Executive Office Armaments and Ammunition. Dr. Jay Clausen and Mr. Christopher Felt, ERDC-CRREL, provided manuscript technical review comments.

COL Teresa A. Schlosser was Commander of ERDC, and Dr. David W. Pittman was the Director.

# Acronyms and Abbreviations

| | |
|---|---|
| BSB | Biogeochemical Sciences Branch |
| C4 | Composition 4 |
| CCDC-AC | Combat Capabilities Development Command Armaments Center |
| CFS | CRREL Fuze Simulator |
| CV | Coefficient of Variance |
| cm | Centimeter |
| CRREL | Cold Regions Research and Engineering Laboratory |
| D10 | Diameter at which 10% of the distribution has smaller particle size |
| D50 | Diameter at which 50% of the distribution has smaller particle size |
| D90 | Diameter at which 90% of the distribution has smaller particle size |
| DNAN | 2,4-Dinitroanisole |
| DoD | Department of Defense |
| ERB | Engineering Resources Branch |
| ERDC | U.S. Army Engineer Research and Development Center |
| ESTCP | Environmental Security Technology Certification Program |
| g | Gram |
| IM | Insensitive Munition |
| LD-PSA | Laser Diffraction Particle Size Analysis |
| LO | Low Order |
| m | Meter |
| mL | Milliliter |
| mm | Millimeter |

| | |
|---|---|
| MPa | Megapascal |
| NTO | Nitrotriazolone |
| oz | Fluid Ounce |
| PE | Polyethylene |
| ProSAir | Propagation of Shocks in Air |
| PSD | Particle-Size Distribution |
| RDX | Hexogen |
| RI | Refractive Index |
| SEPD | Surface Explosives Particles Dispersion Model |
| SERDP | Strategic Environmental Research and Development Program |
| SPB | Signature Physics Branch |
| THz | Terahertz |
| TNT | 2,4,6-Trinitrotoluene |
| TREECS | Training Range Environmental Evaluation and Characterization System |
| μm | Micrometer |

# 1 Introduction

## 1.1 Background

For the Department of Defense (DoD), sustaining military training ranges has become a major concern that requires a detailed understanding of the loading of munitions constituent residues on those ranges. In the past, deposition of munitions constituents (i.e., energetic compounds such as 2,4,6-Trinitrotoluene[TNT], Hexogen [RDX], Nitrotriazolone [NTO], 2,4-Dinitroanisole [DNAN], and others) on ranges was presumed to be predominantly from high-order detonations, as very few rounds were assumed to function improperly (Dauphin and Doyle 2000). Most training-range fate and transport models (i.e., SEPD, ProSAir, and TREECS*) assume this. However, subsequent research found that the most significant readily available source of munitions constituents on impact areas is from munitions that do not function properly, resulting in low-order (LO) detonations (Taylor et al. 2004; M. E. Walsh et al. 2008). Postdetonation particle characteristic data are needed for LO detonation scenarios to inform and constrain models currently used to predict the loading and distribution of munitions constituents on military training ranges.

Table 1 provides general bounds on munition order functioning by the observed efficiency of explosive-filler-mass consumption during detonation and associated residues deposition. The U.S. Army Cold Regions Research and Engineering Laboratory (CRREL) and others developed these descriptors over 20 years of field experimentation and testing through SERDP†-sponsored research projects on residues characterization (ER-1155 [Pennington et al. 2006], ER-1481 [M. R. Walsh, Thiboutot, et al. 2011], and ER-2219 [M. R. Walsh et al. 2017]). These bounds are based on both observations made in the field and measurements of postdetonation material, with the filler-mass consumption efficiencies largely based on conventional (i.e., Composition B and TNT) munitions (e.g., Jenkins et al. 2002; Hewitt et al. 2005; M. R. Walsh, Walsh, Poulin, et al. 2011). High-order detonations of insensitive munitions (IM) tend to have efficiencies

* Surface Explosives Particles Dispersion Model, Propagation of Shocks in Air, and Training Range Environmental Evaluation and Characterization System

† Strategic Environmental Research and Development Program

less than 99.99% (M. R. Walsh, Walsh, Ramsey, Taylor, et al. 2013; M. R. Walsh, Walsh, Ramsey, Brochu, et al. 2013; M. R. Walsh et al. 2018).

Table 1. Detonation characterization descriptors based on conventional munitions.

| Descriptor | Filler Mass Consumed | Munition State |
|---|---|---|
| High-order detonation | 99.99% or more | Total fragmentation |
| Low-order detonation | 75% to 99.98% | Substantial fragmentation with some large pieces |
| Partial detonation | 25% to 75% | Little if any fragmentation with some large pieces |
| Initiated dud | <25% | Fuze gone; intact round with some cracking at nose possible |
| Noninitiated dud | None | Round intact, including fuze |

As high-order detonations typically produce small amounts of very small residual particles (e.g., Taylor et al. 2006) and duds are thought to be relatively intact over decades (Chendorain et al. 2005), LO particles are most relevant to immediate range impacts because of relative mass deposition and availability for mobilization.

The size, shape, spatial distribution, and total mass of particles resulting from LO detonations determine the kinetics and extent of energetic compound dissolution (Taylor et al. 2015). Therefore, they also determine the strain placed on biological systems and the buffering capacity of soils in attenuating the transport of these compounds to surface water and groundwater. Experimental data on the particle characteristics for LO detonations are thus vital in accurately modeling the fate and transport of energetic compounds in conventional and IM high-explosives residues.

Until recently, there was no reliable method of quantifying the particle size of energetics residues from different detonation scenarios or of realistically simulating a LO detonation. Currently the only technique readily available is sieve stack analysis, traditionally used for characterizing geologic material, which relies on relatively coarse bin sizes, resulting in few data points. Headrick (2015) applied laser diffraction particle size analysis (LD-PSA) to energetic materials during the development and manufacturing process but it has yet to be applied to postdetonation material.

## 1.2 Objectives

The goal of this study was to validate the use of LD-PSA on LO particles composed of the IM formula IMX-104 by comparing the results to the conventional sieve stack method.

Specific research objectives were

1. to estimate the Refractive Index (RI) of LO IMX-104 particles,
2. to validate the RI using triplicate analyses of multiple samples, and
3. to compare LD-PSA results to sieve stack data previously compiled for test samples.

## 1.3 Approach

In this study, we used previously collected LO particles from SERDP ER-2219 to validate the use of LD-PSA as a technique for characterizing particle size. RI was determined through the use of the recalculation software on the Horiba LA-960 Laser Diffraction Particle Size Analyzer. This recalculation allowed us to vary the two components of the RI in an iterative recalculation process that reduced error when converting raw data to a particle-size distribution (PSD), commonly known as the R parameter (Horiba 2008a, 2008b, 2014). We then verified the chosen RI through triplicate analyses of multiple samples with the coefficient of variation between those analyses not exceeding the standard outlined in USP <429> (USP 2016).

Once the RI of IMX-104 was estimated, the archived samples were analyzed by LD-PSA and the results compared to PSD data previously collected by sieve stack analysis.

# 2 Methods

## 2.1 March 2015 command-detonation testing and sampling

The command-detonation testing that generated the LO detonation particles analyzed in this project was conducted in March 2015 for SERDP project ER-2219 (M. R. Walsh et al. 2017). The original test objective was to determine the spatial distribution of residues following a LO detonation. The testing munitions consisted of excess 81 mm IMX-104 mortar bodies from manufacturing test runs and were issued with a supplemental charge and no fuze. The rounds used for testing were obtained by the Defence Research and Development Canada–Valcartier from the Combat Capabilities Development Command Armaments Center (CCDC-AC), formerly the Armaments Research, Development, and Engineering Center. Mortar bodies were threaded into 13 Mpa.

$^2$ by 2 cm thick aluminum plates and placed on 30 cm$^2$ by 0.64 cm thick steel plates at detonation points on clean ice. The rounds were command detonated with a CRREL fuze simulator (CFS) with a booster charge of Composition C4 (C4) (M. R. Walsh, Walsh, and Hug 2011). The booster charge was placed in the base of the CFS and threaded into the nose of each round with the original supplemental charge removed (Figure 1).

Figure 1. An 81 mm IMX-104 mortar body with CFS and C4 booster load.

The testing varied the mass of C4 between 7 and 9 g to achieve the LO detonation outcome. Rounds were initiated by a blasting cap inserted through the nose of the CFS into the C4 booster charge at its base. Table 2 summarizes the LO detonation tests carried out during the 2015 field campaign.

Table 2. Low-order detonation tests from March 2015 with estimated detonation type. Adapted from M. R. Walsh et al. (2017).

| Test | Booster Load (C4) | Est. Detonation Type | Samples |
|---|---|---|---|
| LO-1 | 9 g | Low order | Whole area swept and bagged |
| LO-2 | 7 g | Low order | Picked particles and swept annuli |
| LO-3 | 7 g | Partial Detonation | Picked particles and swept annuli |
| LO-4 | 7 g | Fuze only | Picked up a few chunks |
| LO-5 | 7 g | Fuze only | Picked up a few chunks |
| LO-6 | 8 g | Partial detonation | Picked particles and swept annuli |
| LO-7 | 8 g | Low order | Picked particles and swept annuli |

All detonations aside from Test LO-1 were conducted in pairs on two detonation sites 64 m apart (center to center) and 10 m in diameter. Each detonation site consisted of 1 m concentric rings that were measured out from the detonation point and marked with brightly colored paint (Figure 2).

Figure 2. Marking 1 m annuli around the detonation point. Rings were marked in alternating colors.

All samples were swept from the clean ice surface and collected into 38 × 76 cm laboratory-clean polyethylene (PE) bags for future use. Test LO-1 was conducted as an initial test of the detonation and sampling concept and was sampled in its entirety in one whole population sample as there were no particles greater than 1 mm apparent on visual inspection of the detonation plume. For Tests LO-3, -6, and -7, the larger particles and finer residue were swept up from each annulus and put into separate PE bags noting the test detonation (e.g., LO-3) and the distance of the annulus from the point of detonation (e.g., 2–3 m). For LO-2, -3, -6, and -7, particles that were observed beyond the 10 m sampling area were recorded with a GPS, sized and weighed in the field, and collected in plastic containers for further analysis at the field laboratory. Both LO-4 and LO-5 did not initiate the explosive filler and were catalogued as initiated duds. The particles that were ejected from these rounds were collected and placed in plastic containers. Following sample collection, particles were extracted from the mixed particle and ice-fragment matrix in the laboratory by freeze-drying.

## 2.2 Particle isolation

When originally collected, LO particles in the samples were mixed with granular ice generated by the detonation of the rounds and needed to be freeze-dried to isolate the energetic material. This was done with a VirTis Freezemobile 12XL freeze-dryer (Figure 3).

Figure 3. VirTis Freezemobile 12XL freeze-dryer loaded with 2015 particle samples.

Samples were stored and prepared for freeze-drying in a −20°C cold room to avoid melting the ice matrix and potentially dissolving the IMX-104 particles. Samples were split (as needed) and placed into secondary containment vessels, 8 oz glass jars, and topped with filter paper (Melitta M/N 629520 4- to 6-cup white unbleached paper basket-type filter, ≈20 μm pore size) and a ring cap (Figure 4). The Melitta coffee filter served as a secondary filter, in addition to the freeze-dryer vessel's filter, to prevent the loss of fine material through suspension caused by the initiation and release of vacuum pressure.

Figure 4. Top-view of 8 oz jars filled with a split sample and topped with filters and ring caps


Secondary containment vessels were then placed inside 600 mL VirTis freeze-drying bulbs and attached to the Freezemobile 12XL with rubber seals outfitted with an interior filter. The Freezemobile 12XL had a set condenser temperature of −75°C, and samples were left connected for at least 48 hours until all the ice fragments had sublimated into the collection chamber of the freeze-dryer (Figure 5). Once removed, samples were recombined into a single jar for sieve stack analysis.

Figure 5. Detail view of VirTis Freezemobile 12XL with 2015 samples.


## 2.3 Sieve stack analysis

Following freeze-drying and recombining, samples were sieved to determine size fractions. To keep the processing methodology consistent, the same sieve sizes used during field processing of samples, 9.51, 4.5, 2, 1, and 0.5 mm U.S. Standard brass sieves, were used to process samples inside of a fume hood in Hanover, New Hampshire (Figure 6a). To reduce the amount of fragmentation of energetic particles, sieves were shaken by hand as opposed to using a mechanical shaker. During this process, debris, including sticks, seeds, detonation cord plastic sheathing, and metal fragments from the mortar bodies, was removed Figure 6b).

Figure 6. Sieve stack setup in the fume hood and the resulting particle-size fractions and debris.

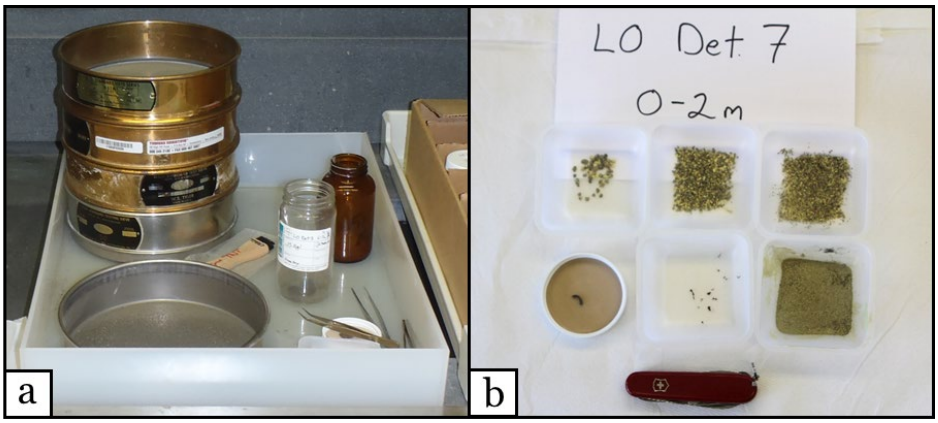

Size fractions were massed and particle counts estimated by massing a subset of particles and back calculating by using the measured mass and the density of IMX-104. Samples were kept in their individual size fractions and refrigerated until needed for further analysis.

## 2.4 Estimation of refractive index

For the purposes of this study, when we refer to the refractive index, we are actually referring to what is known as the complex refractive index (RI), which is defined by

$$n^* = n + ki, \tag{1}$$

where

$n^*$ = the complex refractive index;
$n$ = the real component indicating the phase velocity;
$i$ = the sqrt (–1); and
$k$ = the extinction coefficient, also known as the imaginary component, which is associated with the absorption phenomena or opaqueness of the material (Horiba 2008a).

The selection of an RI in the Horiba LA-960 software is known as an RI kernel and is made up of both the real and imaginary components. To analyze the IMX-104 particles by LD-PSA, the two components of the RI, $n$ and $k$, needed to be determined either through literature research or optical measurement. We found no published values for the RI of IMX-104 for the wavelengths of light used during LD-PSA, so we needed to estimate the RI components by using the Horiba LA-960 software. Even though published values of RI were not available for the wavelengths of interest, Palka and Szala (2016) did measure the RI of melt-cast IMX-104 samples through time domain spectroscopy. They found that for frequencies ranging from 0.1 to 3 THz, bulk IMX-104 samples had calculated refractive indices ranging from approximately 2.1 to 1.85. Although the frequency at which Palka and Szala investigated IMX-104 would correspond to a much larger wavelength than those utilized in LD-PSA, we could use the range of RI values they calculated as a reference point for our estimation of the RI.

The Horiba software includes a calculation that quantifies the quality of raw data and resulting PSD for a selected RI kernel. This measure of quality is given by the residual R parameter defined by

$$R = \frac{1}{N}\sum_{i=1}^{N}\left\{\frac{1}{y_{(x_i)}}\right\}|y_i - y(x_i)|, \quad (2)$$

where

$N$ = the number of detectors used for the calculation;
$y_i$ = the measured scattered light at each channel of the detector; and
$y(x_i)$ = the calculated scattered light at each detector, based on the RI kernel used and the PSD (Horiba 2008b).

By systematically varying each component and zeroing in on the lowest R parameter, the error of the resulting calculation can be reduced and the most appropriate RI components chosen for the "unknown" material. To confirm the RI as being appropriate for the material, we ran the test samples in triplicate and calculated a coefficient of variance (CV) for each triplicate set. Confirmation of the estimated RI used the CV metric for D10, D50, and D90 (i.e., diameters at which 10%, 50%, and 90% of particles are smaller) of 15%, 10%, and 15%, respectively, following the USP <429> standard for light diffraction methods of particle size (USP 2016).

## 2.5 Laser diffraction particle size analysis

Following estimation of the RI components for IMX-104, the Horiba LA-960 was used to process the archived LO particles from LO-2, -3, -6, and -7. To allow recovery of sample material, a Nilfisk 118EXP explosion-proof vacuum was attached to the system. The suction flow of the 118EXP was reduced to the same settings as the original Nilfisk GM 80 factory settings with the use of a variable speed controller. Samples were first sieved so that the size fraction greater than 2 mm was removed to avoid clogging the intake and flow cell of the instrument. An initial sample mass was taken and the sample loaded into the sample chute for analysis. Samples were run on automatic feeder settings with the forced air pressure set to 0.32 MPa and sample data acquisition times set to 50000 (50 seconds). A low forced air pressure setting was used to avoid breaking particles during the analysis process. For most samples (>~3 g), it was necessary to conduct multiple analyses for all material to pass through the analyzer. Following sample analysis, the filter of the Nilfisk 118EXP was shaken out into the stainless steel collection chamber, and the sample was recovered

using static-free brushes. Samples were run in triplicate, and the instrument was cleaned after triplicate analyses by running Ottawa sand through the analyzer to avoid cross contamination between samples.

Following analysis, each sample had multiple output data files with volumetric PSDs that were averaged to produce the compiled PSD for each sample. The sieve stack process creates a PSD based on mass, and the LD-PSA methodology creates a PSD based on sample volume. Since the material being analyzed in this case was uniform in density, there was no need to convert between mass and volume distributions (Horiba 2005). Both PSDs and percent cumulative results of each analyzed sample were used for comparison.

# 3 Results and Discussion

## 3.1 Sieve stack analysis

The total mass of particles was calculated after freeze-drying and was used to calculate detonation efficiency (Table 3). The detonation results are based on recovered particles and observations made of round fragmentation. In the case of LO-7, we classified this round as a LO detonation and not a partial detonation because the round was substantially fragmented and recovered residues were close to the LO range of values given in Table 1.

Table 3. Detonation results from low-order detonation tests, March 2015. Adapted from M. R. Walsh et al. (2017).

| Test | Booster (C4) | Result | Recovered Residues[a] | Overall Efficiency[b] |
|---|---|---|---|---|
| LO-1 | 9 g | Low order | 20% | 80% |
| LO-2 | 7 g | Partial detonation | 30% | 20%[d] |
| LO-3 | 7 g | Low order | 6%[e] | 94% |
| LO-4 | 7 g | Dud (fuze only) | 2%[c] | 0.9% |
| LO-5 | 7 g | Dud (fuze only) | 7%[c] | 0.9% |
| LO-6 | 8 g | Partial detonation | 27%[c] | 20%[d] |
| LO-7 | 8 g | Low order | 31% | 69% |

[a] Percent of original mass recovered as particles.

[b] For partial detonations, filler in the round is estimated. For duds, only booster charge (fuze) detonated.

[c] Particles recovered only outside the body of the round. Total energetics remaining is in the 99% range.

[d] Estimate based on recovered residues plus estimate of remaining explosive filler in the round.

[e] Includes estimate of residues in samples lost during desiccation process.

Of the seven rounds detonated during the March 2015 tests, only three rounds, LO-1, -3, and -7, detonated LO and two, LO-2 and -6, were partial detonations. As noted earlier, LO-4 and -5 were initiated duds; and the material from LO-1 was swept, melted, and analyzed by HPLC. Therefore, the detonation material investigated for this study was from LO-2, -3, -6, and -7. Because of the varying efficiencies, we present the partial and LO results separately.

### 3.1.1 Low-order detonations

The majority of particles from LO-3 and -7 were less than 0.5 mm in size. For LO-3, this accounts for 50.8% of the freeze-dried sample, 9.6 g of the total 18.8 g sample mass. For LO-7, 58.1% of the total sample mass was less than 0.5 mm, 83.6 g of the 143.9 g sample. It is important to note that

although the total masses differ by an order of magnitude, the majority of the deposited particles for both detonations are less than 0.5 mm in size. Table 4 and Table 5 give the results. No corrections were made to the data for the samples from LO-3 that were compromised (3, 4, and 5 m annuli) during the freeze-drying process.

Table 4. Distribution statistics for LO-3 and -7 based on sieve size.

| Sieve Size (mm) | LO-3 | | LO-7 | |
|---|---|---|---|---|
| | Percent of Total | Total in Bin (g) | Percent of Total | Total in Bin (g) |
| >9.5 | 0% | 0 | 0% | 0 |
| 4.75–9.5 | 0% | 0 | 0% | 0 |
| 2–4.75 | 2.6% | 0.5 | 2.4% | 3.5 |
| 1–2 | 24.3% | 4.6 | 16.0% | 23.0 |
| 0.5–1 | 22.2% | 4.2 | 23.5% | 33.8 |
| <0.5 | 50.8% | 9.6 | 58.1% | 83.6 |
| *Total* | *100%* | *18.9* | *100%* | *143.9* |

Table 5. Distribution statistics for LO-3 and -7 based on annuli distance.

| Annulus Distance (m) | LO-3 | | LO-7 | |
|---|---|---|---|---|
| | Percent of Total | Total in Bin (g) | Percent of Total | Total in Bin (g) |
| 0–2 | 14.3% | 2.7 | 7.4% | 10.6 |
| 2–3 | 16.9% | 3.2 | 16.7% | 24.0 |
| 3–4 | * | * | 13.8% | 19.8 |
| 4–5 | * | * | 15.1% | 21.7 |
| 5–6 | * | * | 11.3% | 16.3 |
| 6–7 | 25.9% | 4.9 | 12.2% | 17.5 |
| 7–8 | 14.8% | 2.8 | 8.6% | 12.4 |
| 8–9 | 10.6% | 2.0 | 9.7% | 14.0 |
| 9–10 | 17.5% | 3.3 | 5.3% | 7.6 |
| *Total* | *100%* | *18.9* | *100%* | *143.9* |

* Particles for these annuli were lost for LO-3 during the freeze-drying process when the samples melted due to a filter blockage.

### 3.1.2 Partial detonations

The majority of particles from LO-2 and -6 were also found to be less than 0.5 mm in size. For LO-2, this accounts for 63.0% of the freeze-dried sample, 195.1 g of the total 309.5 g sample mass. For LO-6, 58.6% of the total sample mass, or 30.3 g of the 51.7 g sample, was found to be less than 0.5 mm. As was found with LO-3 and -7, even though these two samples

differ in mass by one order of magnitude, the majority of the deposited particles from the freeze-dried portion are less than 0.5 mm in size. Table 6 and Table 7 show these results.

Table 6. Distribution statistics for LO-2 and -6 based on sieve size.

| Sieve Size (mm) | LO-2 | | LO-6 | |
|---|---|---|---|---|
| | Percent of Total | Total in Bin (g) | Percent of Total | Total in Bin (g) |
| >9.5 | 0% | 0 | 0% | 0 |
| 4.75–9.5 | 0% | 0 | 0.2% | 0.1 |
| 2–4.75 | 2.1% | 6.6 | 2.5% | 1.3 |
| 1–2 | 13.8% | 42.8 | 10.3% | 5.3 |
| 0.5–1 | 21.0% | 65.0 | 28.4% | 14.7 |
| <0.5 | 63.0% | 195.1 | 58.6% | 30.3 |
| *Total* | *100%* | *309.5* | *100%* | *51.7* |

Table 7. Distribution statistics for LO-2 and -6 based on annuli distance.

| Annulus Distance (m) | LO-2 | | LO-6 | |
|---|---|---|---|---|
| | Percent of Total | Total in Bin (g) | Percent of Total | Total in Bin (g) |
| 0–1 | 35.7% | 110.4 | 46.5% | 24.1 |
| 1–2 | 8.0% | 24.8 | | |
| 2–3 | 16.1% | 49.9 | 16.0% | 8.3 |
| 3–4 | 16.5% | 51.2 | 13.5% | 7.0 |
| 4–5 | 6.7% | 20.7 | 12.5% | 6.5 |
| 5–6 | 4.1% | 12.6 | 3.9% | 2.0 |
| 6–7 | 3.6% | 11.1 | 5.8% | 3.0 |
| 7–8 | 2.7% | 8.5 | 1.7% | 0.9 |
| 8–9 | 3.8% | 11.7 | 0% | 0 |
| 9–10 | 2.8% | 8.6 | 0% | 0 |
| *Total* | *100%* | *309.5* | *100%* | *51.7* |

## 3.2 Estimation of refractive index using the Horiba LA-960

The first step of estimating the RI for IMX-104 was to analyze a sample on the Horiba LA-960 and then to recalculate the results with new RI kernels, varying both the real and imaginary components. We chose LO-2 0–2 m for this estimation, referred to as LO-2 for the rest of this section. Initially, LO-2 was recalculated with a real component of 1, 2, 3, 4, and 5 and imaginary components for each of 0.01, 0.1, 1, 5, and 10 (equation 1). These

were used to evaluate the real and imaginary components over a wide range of values. By doing so, the investigative window was narrowed by finding the lowest nonzero R parameters in this range. Table 8 summarizes the results of this first step.

Table 8. Summary of R parameter data for step one of the RI estimation for LO-2 particle analysis.

| Real Component ($n$) | Imaginary Component ($k$) | R Parameter | Real Component ($n$) | Imaginary Component ($k$) | R Parameter |
|---|---|---|---|---|---|
| 1 | 0.01 | 0.11569 | 4 | 0.01 | 0.047424 |
| 1 | 0.1 | 0 | 4 | 0.1 | 0 |
| 1 | 1 | 0.047717 | 4 | 1 | 0.048143 |
| 1 | 5 | 0 | 4 | 5 | 0 |
| 1 | 10 | 0 | 4 | 10 | 0 |
| 2 | 0.01 | 0.04565 | 5 | 0.01 | 0.047566 |
| 2 | 0.1 | 0.046937 | 5 | 0.1 | 0 |
| 2 | 1 | 0.047897 | 5 | 1 | 0.047994 |
| 2 | 5 | 0 | 5 | 5 | 0 |
| 2 | 10 | 0 | 5 | 10 | 0 |
| 3 | 0.01 | 0.047127 | | | |
| 3 | 0.1 | 0 | | | |
| 3 | 1 | 0.048306 | | | |
| 3 | 5 | 0 | | | |
| 3 | 10 | 0 | | | |

As seen in Table 8, the lowest nonzero R parameters were returned for an imaginary component of 1 and 0.1. The lowest R parameter corresponding to imaginary components of 1 and 0.1 were for real components with values of 1 and 2, respectively. These values are near or in the original window targeted for investigation based on Palka and Szala (2016), which provided further support for these determined values. The second step of this investigation was to estimate the imaginary component by recalculating the original LO-2 particle-size dataset with fixed real component values of 1 and 2. For each of these real component values, the imaginary component values for each were varied from 0.95 to 0.99 and 0 to 0.07, respectively. The imaginary components were varied in increments of 0.01. Figure 7 and Figure 8 show the results.

Figure 7. Parameters for RI 1 and imaginary components ranging from 0.95 to 0.99.

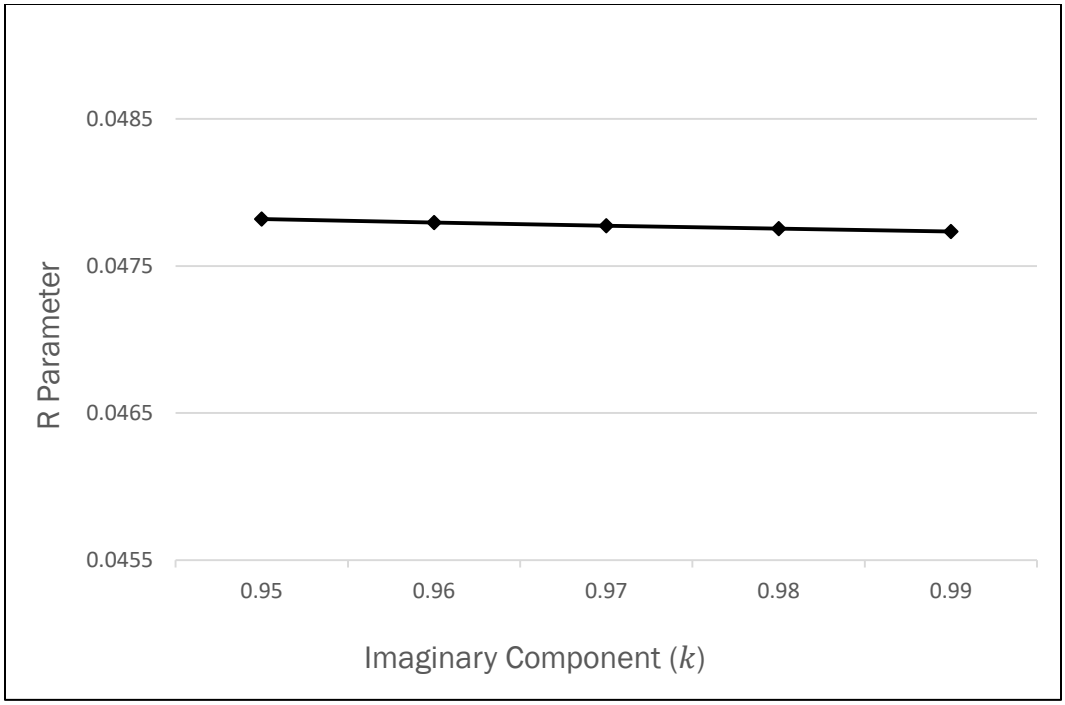


Figure 8. R parameters for RI 2 and imaginary components ranging from 0 to 0.6 (0.7 is not shown because it returned a value of 0).

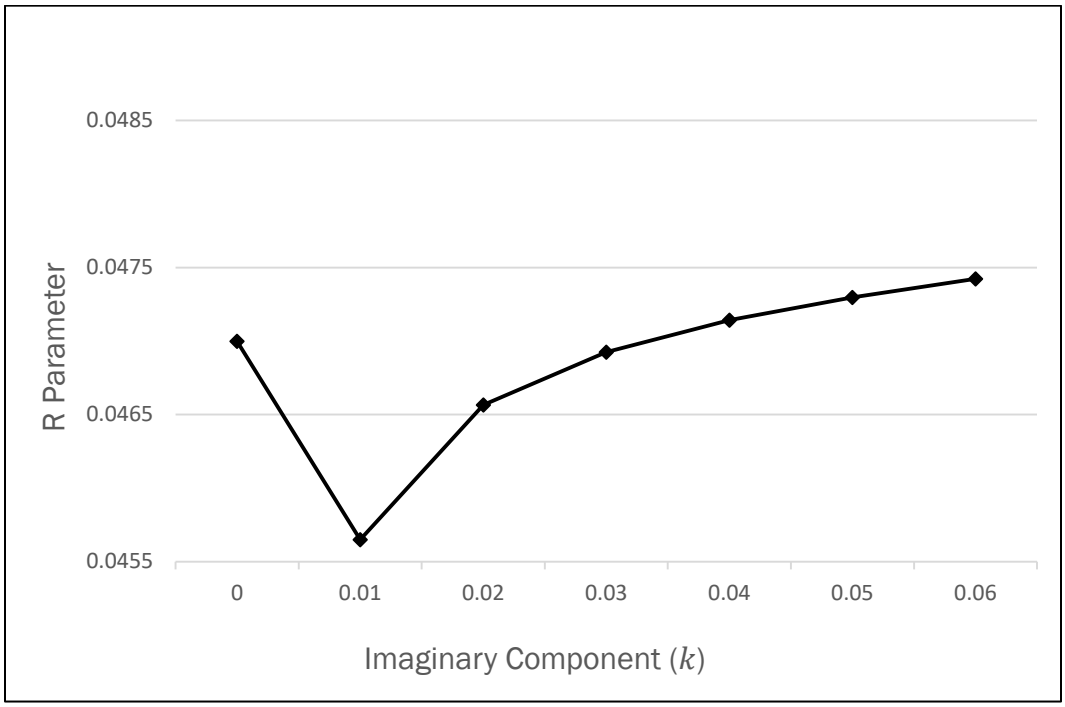


As seen in Figure 7 and Figure 8, the lowest resulting imaginary component was 0.01 for a real component of 2. The third step in calculating the RI kernel was to take the newly determined fixed imaginary component value of

0.01 and recalculate the R parameter for a range of real component values from 1.5 to 2.5 in increments of 0.05. The results of this recalculation determine the RI to the second decimal place (Figure 9 and Figure 10).

Figure 9. R parameters for RI of 1.5–2.5 with a fixed imaginary component of 0.01.

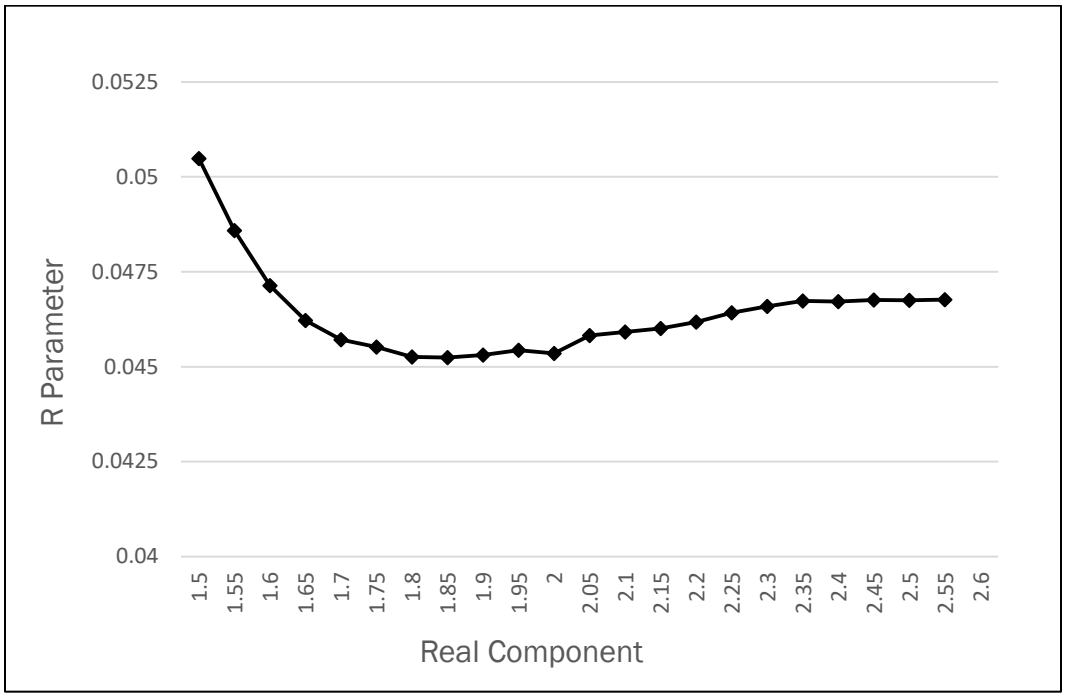


Figure 10. Detail view of the lowest R parameter data for RI of 1.5–2.5 with a fixed imaginary component of 0.01.

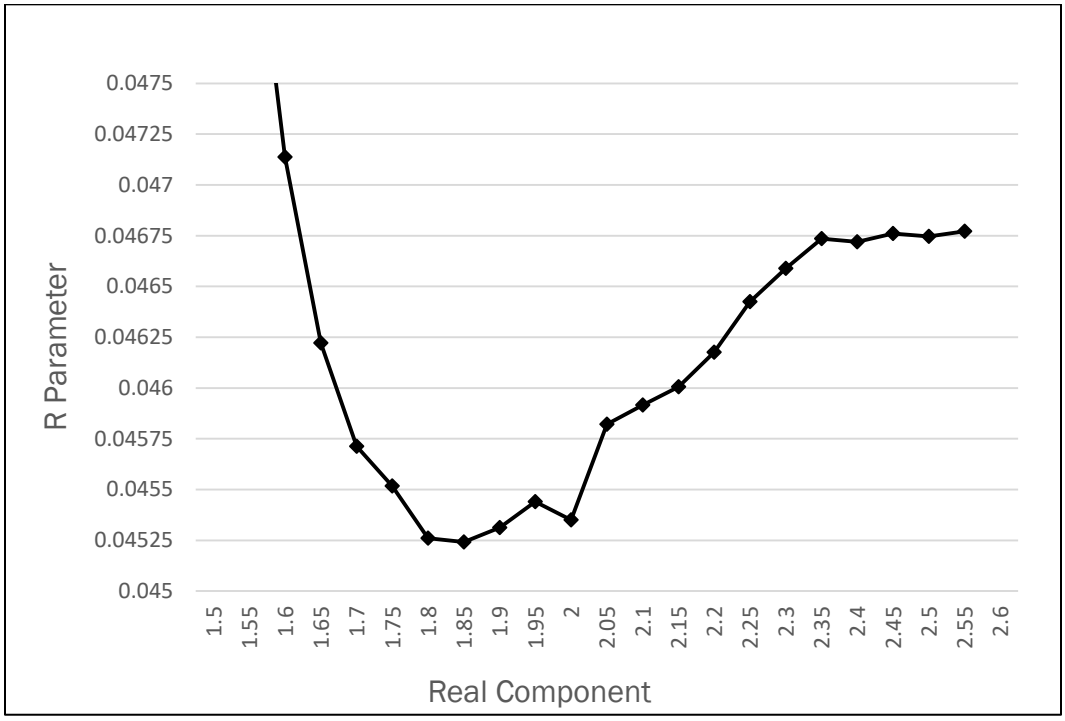

As seen in Figure 10, the lowest R parameter value was found for a refractive index real component of 1.85. The fourth and final step determined the RI kernel to the third decimal place. Although for most applications the RI needs to be determined to the second decimal place only, we chose this approach based on consultation with the manufacturer of our analyzer. We accomplished this fourth step by performing a similar analysis as step three described above. The RI imaginary component was held constant at 0.01, and the RI real component was varied from 1.800 to 1.905 by increments of 0.005. Figure 11 shows the results of this fourth step.

Figure 11. Detail view of the lowest R parameter data for RI of 1.800–1.905 with a fixed imaginary component of 0.01.

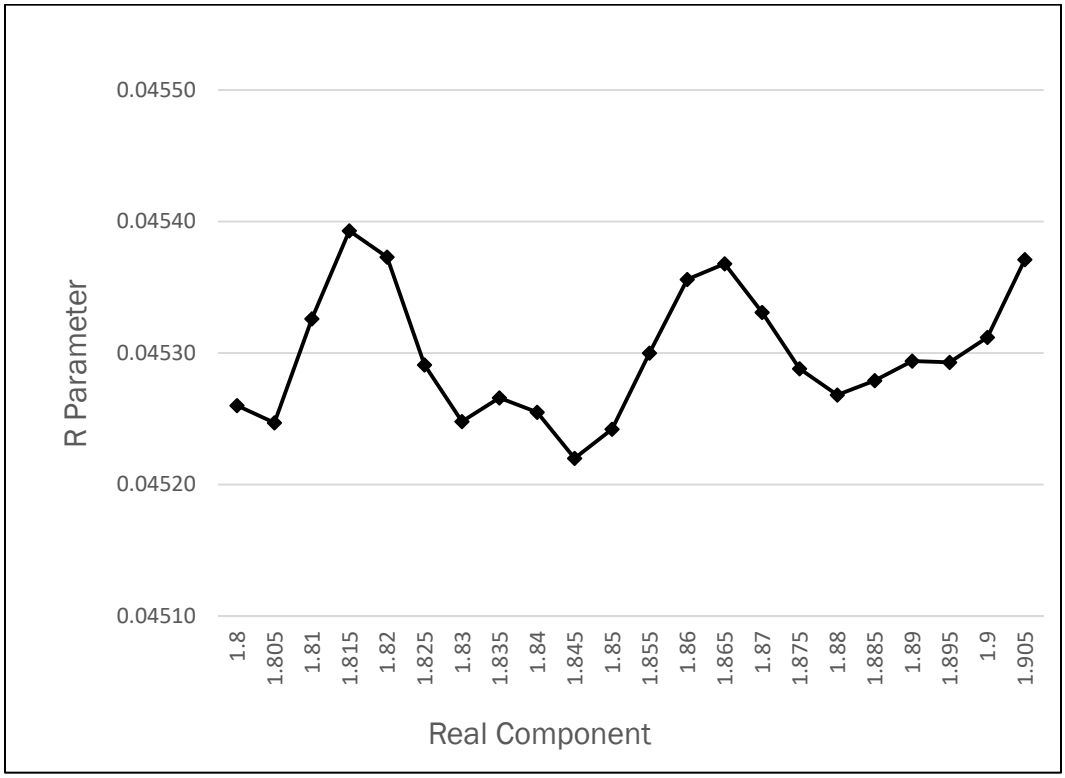


Through this four-step iterative process, the resulting RI kernel determined for IMX-104 was 1.845 ($n$) with an imaginary component ($k$) of 0.01, notated as 1.845 0.01$i$ as originally depicted in equation (1). This RI kernel value was then used on triplicate analyses of all samples from LO-2, -3, -6, and -7. The results of these analyses were then compiled and CVs computed for each. Table 9 shows that approximately half of the samples used for confirmation passed the USP <429> D10, D50, and D90 standard of less than 15%, 10%, and 15%, respectively (USP 2016).

Table 9. Summary of CV values calculated for triplicate runs of LO-2, -3, -6, and -7.

| Sample ID | CV | | |
|---|---|---|---|
| | D10 | D50 | D90 |
| *LO-2 0–1 m*[a] | - | - | - |
| LO-2 1–2 m | 23.9 | 18.9 | 18.1 |
| LO-2 2–3 m | 5.1 | 12.1 | 8.9 |
| LO-2 3–4 m | 13.7 | 9.9 | 6.9 |
| LO-2 4–5 m | 30.7 | 11.0 | 8.0 |
| LO-2 5–6 m | 43.7 | 12.7 | 12.1 |
| LO-2 6–7 m | 7.5 | 3.5 | 7.9 |
| LO-2 7–8 m | 15.2 | 21.0 | 18.8 |
| LO-2 8–9 m | 21.4 | 12.1 | 5.1 |
| LO-2 9–10 m | 12.8 | 18.4 | 3.9 |
| LO-3 Whole Population[b] | 2.1 | 0.5 | 1.1 |
| LO-6 0–2 m | 23.1 | 14.2 | 9.7 |
| LO-6 2–3 m | 36.7 | 22.9 | 10.6 |
| LO-6 3–4 m | 8.9 | 2.8 | 2.7 |
| LO-6 4–5 m | 3.4 | 1.7 | 1.9 |
| LO-6 5–6 & 7–8 m[c] | 12.3 | 9.8 | 3.7 |
| LO-6 6–7 m | 12.3 | 8.5 | 0.4 |
| LO-7 0–2 m | 9.4 | 12.9 | 4.8 |
| LO-7 2–3 m | 23.9 | 3.0 | 0.4 |
| LO-7 3–4 m | 20.5 | 7.4 | 4.8 |
| LO-7 4–5 m | 9.3 | 1.9 | 3.4 |
| LO-7 5–6 m | 12.0 | 7.9 | 3.9 |
| LO-7 6–7 m | 13.3 | 6.0 | 6.3 |
| LO-7 7–8 m | 14.0 | 4.0 | 3.7 |
| LO-7 8–9 m | 8.6 | 2.6 | 2.2 |
| LO-7 9–10 m | 18.0 | 9.3 | 3.3 |

[a] LO-2 0–1 m not judged against the CV standard as it was the sample used to estimate the RI kernel.

[b] Annuli combined, not enough mass to run individually; does not include 3, 4, and 5 m samples.

[c] Annuli combined, not enough mass to run individually.

In Table 9, the majority of the samples that did not pass the CV standard, 9 of 13, had increasing CV values with lower estimated particle-size diameter. To better understand this phenomenon, the PSDs for each of the triplicate runs were plotted together to examine changes in PSD with each successive analysis (Figure 12; Appendix A and Appendix B).

Figure 12. PSD plots of LO particle samples with the highest change in CV for D10 and D50.

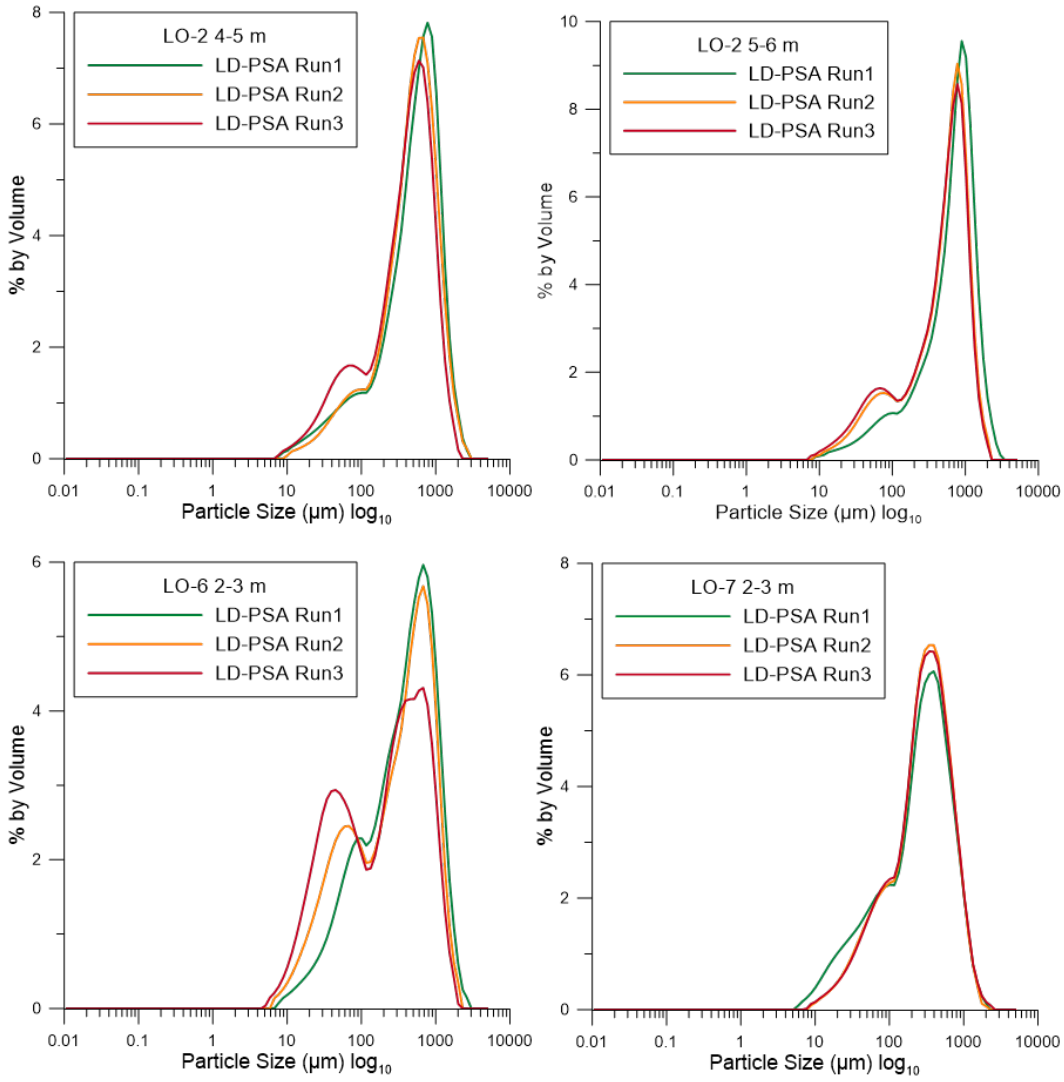


Figure 12 depicts the PSD results of the four samples with the highest change in CV for D10 and D50. Although the shape of the PSD stays relatively similar for each of the four samples, there is a marked change that can be observed on each plot for the finer-particle-size material (<200 µm). In this area, every plot, aside from LO-7 2–3 m, shows an increase from Run 1 to Runs 2 and 3 in the percentage of the sample by volume that is made up of this finer material. For sample LO-7 2–3 m, the change in PSD takes place on the largest peak of the plot, and the area under the Run 2 and 3 curves increases the greatest to the left of the maximum value. Similar patterns are seen in the rest of the nonpassing samples, which are included in Appendix A. These observations indicate that the sample is becoming finer with every successive run through the analyzer. This is most pronounced for sample LO-6 2–3 m, where the finer peak of the bimodal

plot grows with every successive run. This observation suggests that after the sample passes the flow cell, the material is breaking down as it travels through the vacuum hose and into the collection chamber of the Nilfisk 118EXP. To further investigate this observation, we compiled the D10, D50, D90, and mean particle sizes for Runs 1, 2, and 3 for all CV analyses that did not pass the standard (Figures 13–16; Appendix A).

Figure 13. Bar plot of LO-2 samples that did not pass the CV standard with a reduction in D10, D50, D90, and mean particle-size values. The full table of values is in Appendix A.

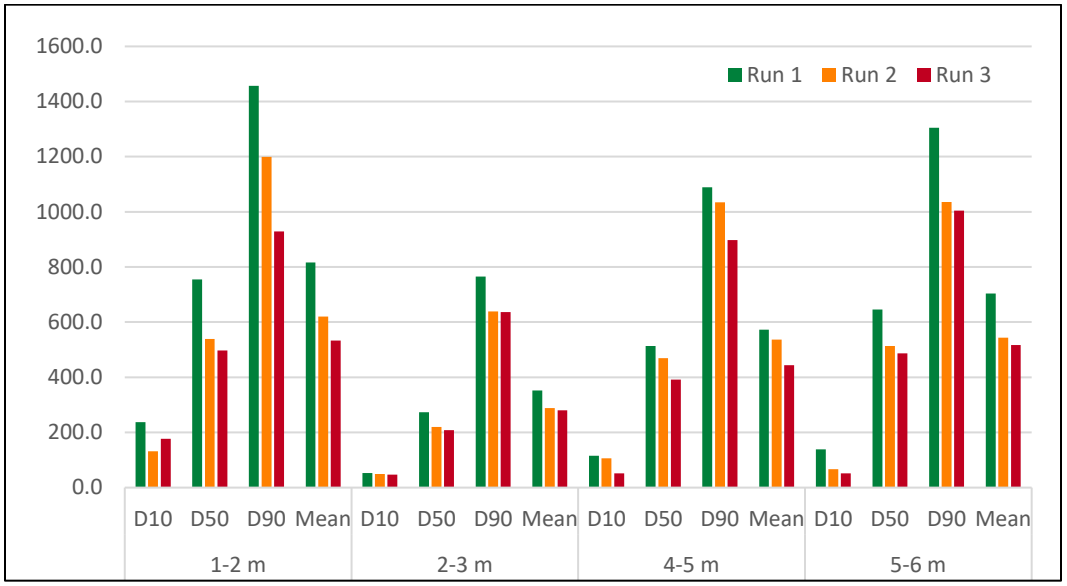


Figure 14. Bar plot of LO-2 samples that did not pass the CV standard with varying change in D10, D50, D90, and mean particle-size values. The full table of values is in Appendix A.

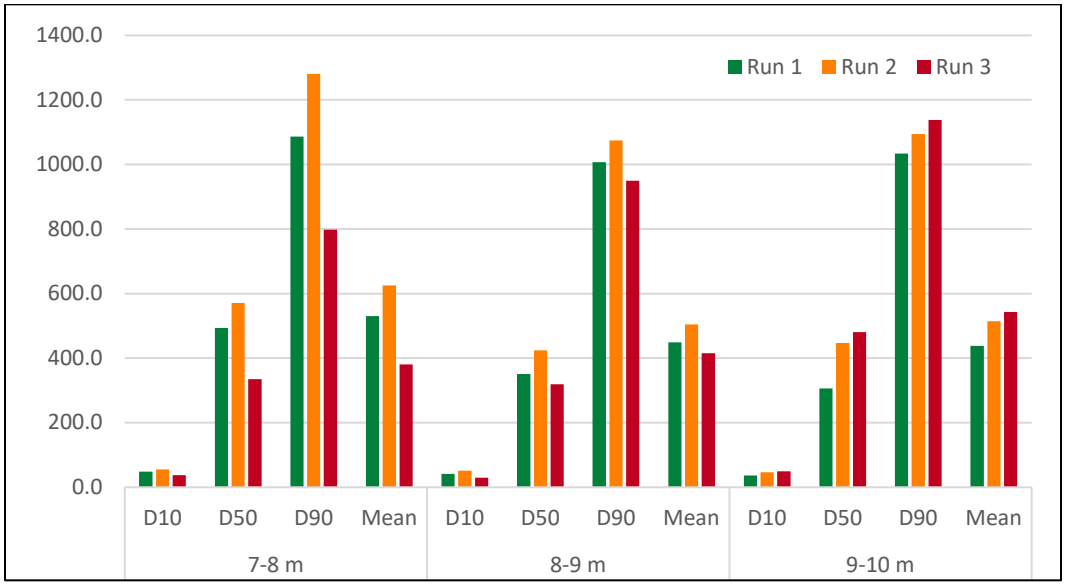

Figure 15. Bar plot of LO-6 samples that did not pass the CV standard with decreasing D10, D50, D90, and mean particle-size values. The full table of values is in Appendix A.

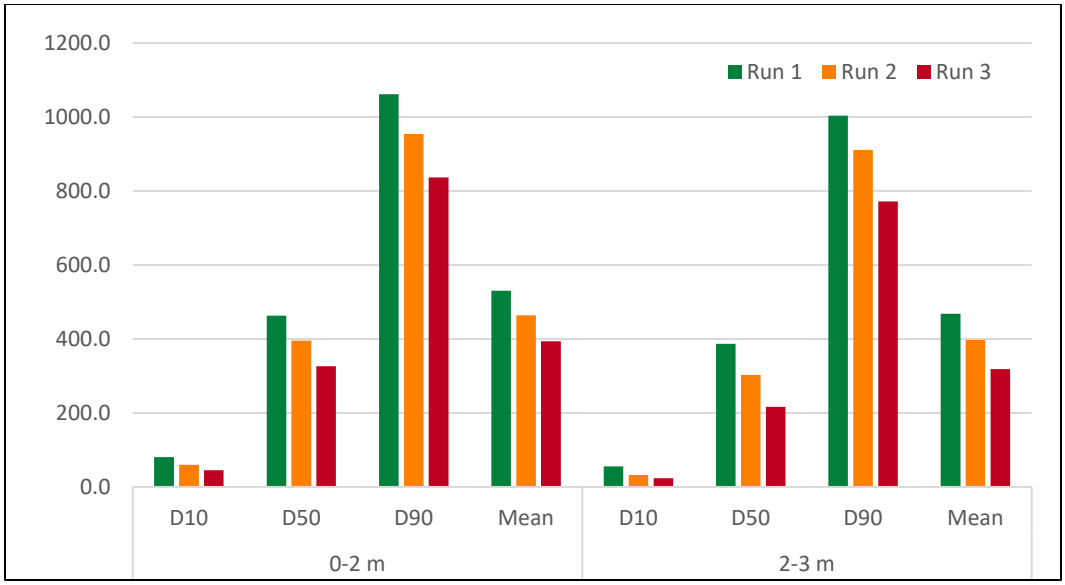


Figure 16. Bar Plot of LO-7 samples that did not pass the CV standard with varying change in D10, D50, D90, and mean particle size. The full table of values is in Appendix A.

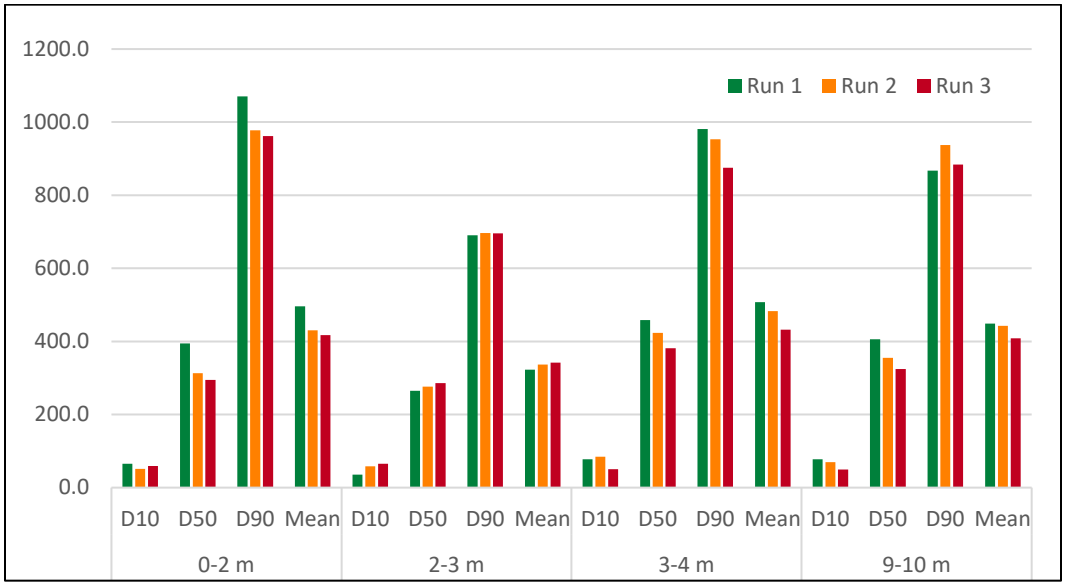


In Figures 13–16, 5 of 13 nonpassing samples saw a reduction in particle size from Run 1 to Run 3 across all four variables, 4 of the 13 samples saw a reduction of three out of four variables, and four samples did not have a reduction in particle size for any of the variables. Based on the PSD plots and the measured reduction in particle size for the majority of measured variables for 9 of 13 samples that were rerun on the LA-960, it became clear that the nonpassing CV values could be caused in part by samples becoming finer with successive runs. There is clearly another factor at work

with samples LO-2 7–8, 8–9, and 9–10 m and LO-7 2–3 m, which showed no consistent reduction in particle size. Of these four samples, only LO-2 7–8 m did not have passing CV values for D10, D50, or D90 (Figure 14; Appendix A). Two of the remaining three samples, LO-2 9–10 m and LO-7 2–3 m, had nonpassing CV values for D50 and D10, respectively. The remaining sample had nonpassing CV values for D10 and D50. These three samples all had passing CV values for D90, which means that the bulk of the material is largely unchanged. However, it is possible that the D90, representing a particle size for 90% of the sample, is unchanged overall but that the reduction in size of several large particles created material that skewed the values for D50 and D10. This effect could also be a factor in why some samples (e.g., LO-2 1–2 m and LO-7 0–2 and 3–4 m) had a reduction in D50 and D90 and increase in D10. This effect, however, would not explain the particle-size change in LO-2 7–8 m.

Another factor that we are continuing to investigate is the potential holdover of material in the sample collection system that can potentially be mixed with subsequent samples. Without additional information, the exact reason for these four nonpassing samples cannot be fully understood. For this study, because of the passing CV values for half of the triplicate runs and the reduction in particle size observed in 9 of the remaining 13 samples, the estimated RI kernel of 1.845 0.01*i* was deemed suitable for continued analysis of IMX-104 particles in future studies. Because of the reduction in particle size observed during the estimation and validation of the RI kernel, only the Run 1 data from every sample are presented here and compared to the sieve stack results.

## 3.3 Laser diffraction particle size analysis

A total of 26 samples were processed by LD-PSA using a Horiba LA-960. Figure 17 presents the compiled PSDs for LO-2, -3, -6, and -7; and Appendix D analyzes each individually. Each sample took approximately 20 minutes to process through the analyzer and to collect the material from the vacuum chamber for future analysis. Sample processing times increased for samples of larger mass as they required additional runs to completely analyze all of the sample material. The largest tested sample was LO-2 0–1 m, which required 18 separate runs.

Figure 17. PSDs for LO-2, -3, -6, and -7 as measured by the Horiba LA-960.

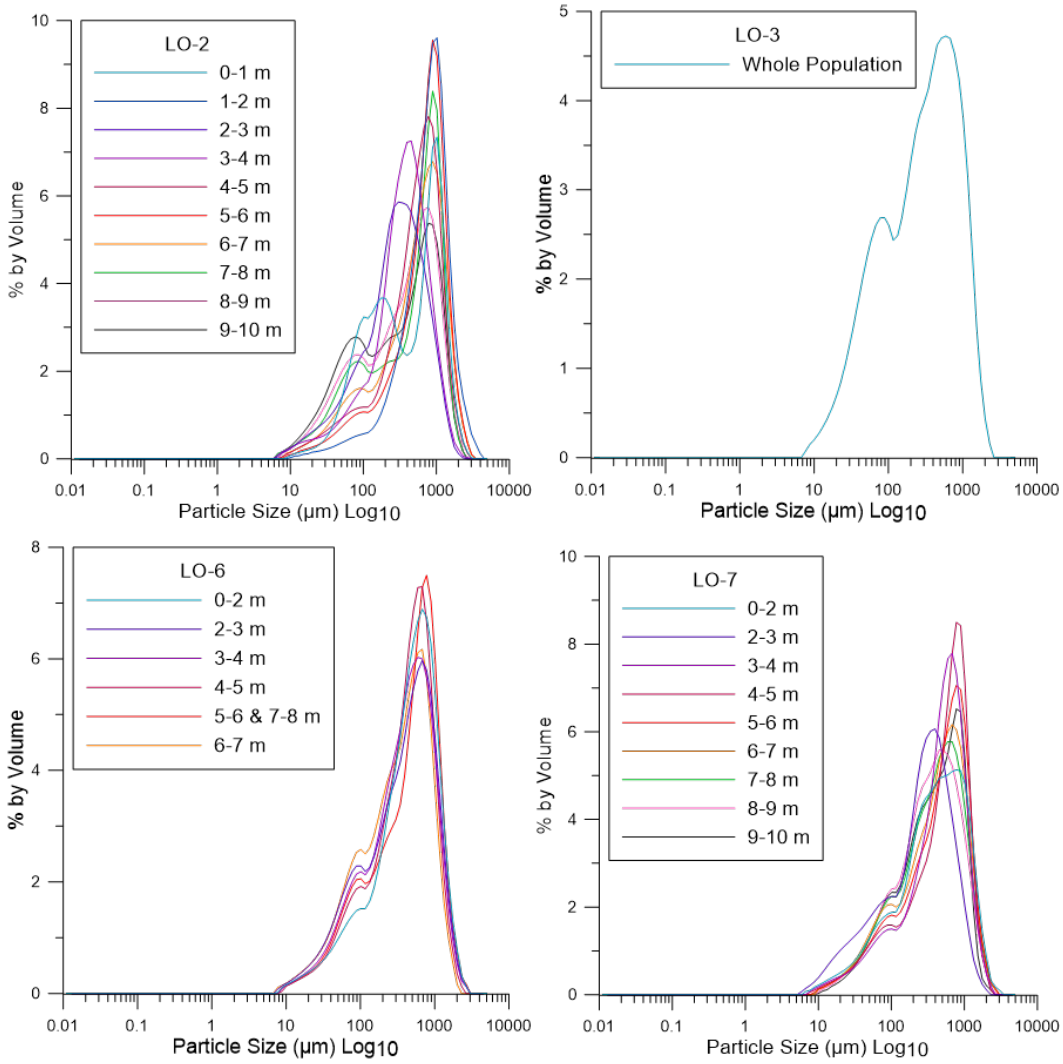


As seen in Figure 17 and Appendix D, the PSD of LO-2 is strongly bimodal in the 0–2 m annulus; and from 6 to 10 m, the particle distribution becomes increasingly bimodal with greater distance from the point of detonation. The PSDs from 2–6 m for LO-2 consist of strong peaks that center over 1 mm in particle size. The PSD for the LO-3 whole population sample is a wide bimodal peak. The maximum value centers over approximately 500 µm with the secondary peak centered around 80 µm. This agrees with the mass data from the sieve stack analysis, indicating the majority of the material is less than 500 µm. When examining the data from LO-6, there is a clear bimodal PSD for all annuli, which becomes stronger beyond 2 m from the point of detonation with a greater percentage of smaller particles. The PSD data from LO-7 are made up of broad peaks that skew to particle sizes less than 1 mm. The PSDs for all samples show good agreement with

one another and tend to be bimodal with peaks centering over roughly 500–1000 μm and 50–100 μm. The bimodal nature of most samples raises an interesting question regarding the composition of different particle-size classes. Does the composition of a sample with a strong secondary peak differ in comparison to a sample with a weaker secondary peak or no secondary peak? As discussed in Dontsova et al. (2014), NTO crystals found in IMX-104 vary in size approximately 300–500 μm, and DNAN particles tend to abrade easily. It is possible that the primary peak is composed of NTO crystals and intact particles of IMX-104 bulk composition and that the finer material is made up of abraded DNAN and finer RDX crystals. Although our study did not investigate this, the chemical composition of postdetonation LO particulate material warrants future research.

## 3.4 Sieve stack and LD-PSA comparison

To compare the sieve stack data to the LD-PSA data, we used the cumulative percent of each dataset. Normally when comparing percent by mass and percent by volume of mixed materials, the mass percentage must be converted into percent by volume using the density of the material. When this comparison is made for mixed materials, this conversion can be difficult because of the varying density of the individual components of the material. However, when comparing these measures for a material of uniform density, as done here, the volume- and mass-based distributions are equal and can be directly compared without conversion (Horiba 2005). This allows the comparison of the sieve stack data, which is based on sample mass, to the LD-PSA data, which is based on sample volume. As presented in section 3.1, the sieve stack data covers a size range of less than 0.5 mm to greater than 9.51 mm as opposed to the LD-PSA methodology, which measures material less than 2 mm only. It is important to note that the Horiba LA-960 can measure particles 5 mm and less; but this study analyzed material that passed through a 2 mm sieve only to avoid potential clogging of the flow cell by elongate particles. This means that, for comparison, only the less than 0.5, 0.5–1, and 2 mm bin sizes from the sieve stack analyses will be compared to the LD-PSA results. Figure 18 shows from each detonation one sample that had the highest CV values for the LD-PSA triplicate analysis compared to its companion dataset from sieve stack analysis (Appendix C).

Figure 18. Step graphs of the cumulative percent by mass of sieve stack data overlain by cumulative percent by volume curves from LD-PSA from the same samples.

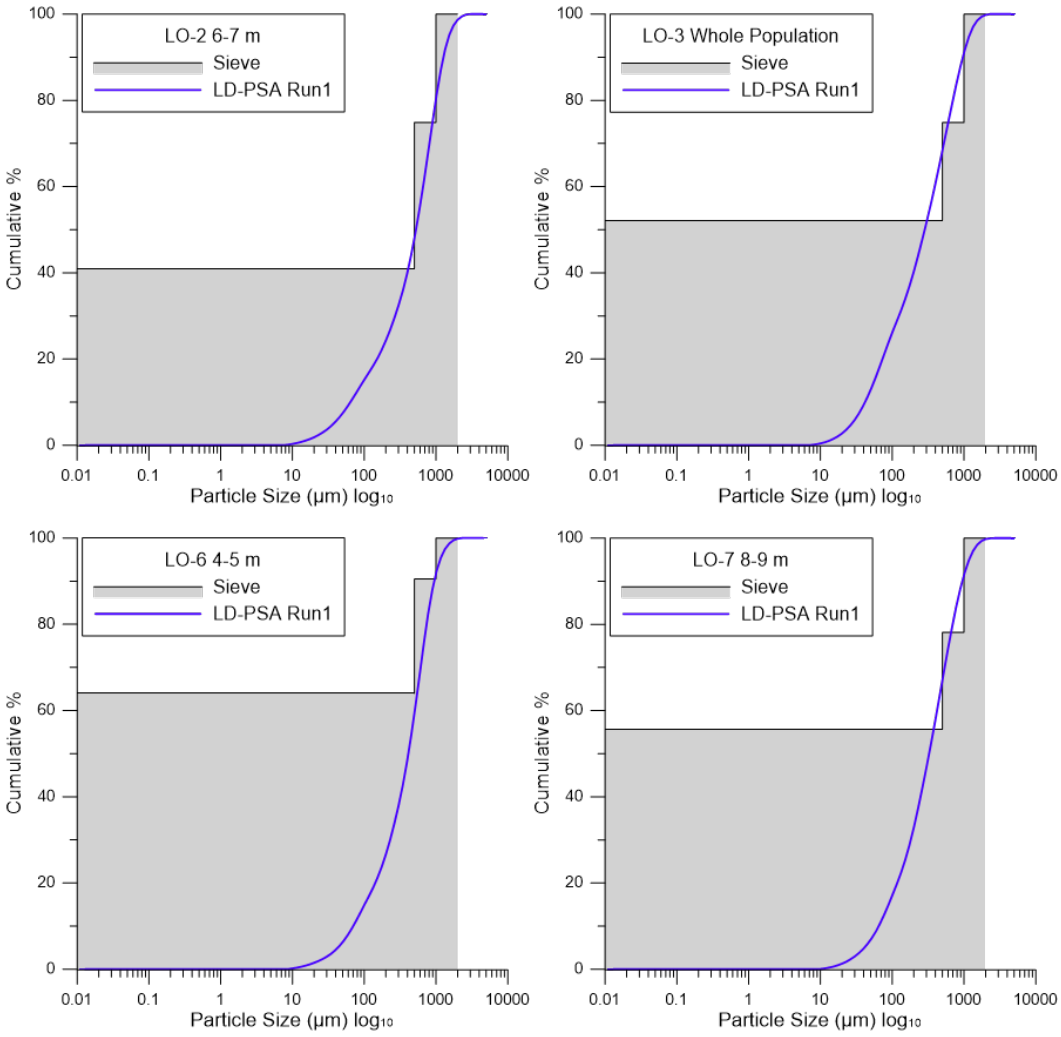


As seen in Figure 18 and the rest of the comparison plots in Appendix D, there is good visual agreement between the cumulative percent curve of the LD-PSA analysis and the step graph presenting the cumulative percent of the sieve stack analyses. The cumulative percent LD-PSA curve does overlap every step in bin size. When directly comparing the cumulative percentages for each relative bin size between the LD-PSA and sieve stack results, there was a maximum difference of 17.4% for less than 0.5 mm, 21.9% for 0.5–1 mm, and 3.4% for 1–2 mm. There was an average difference of 7.7%, 7.8%, and 0.4% and median difference of 7.2%, 5.3%, and 0.2% for each of the three bin sizes, respectively (Appendix E).

Even though there is good agreement between these plots, it is also clear that the LD-PSA results are much more highly resolved. As mentioned in

section 3.3, the output results of the Horiba LA-960 are made up of 50 data points covering the full measurement range of the instrument in dry analysis mode (0.1–5000 μm). Sample processing time is also an important factor when considering which methodology is most appropriate to use. When processing a sample by hand, it typically took 1–1.5 hours per sample to completely sieve, mass, and catalog each sample, compared to the 20 minutes it takes to run a sample through the laser diffraction particle size analyzer and recollect the material from the vacuum collection chamber. The LD-PSA methodology is easily the faster of the two methods when used alone.

# 4 Conclusions

Based on our investigation of IMX-104 by using the Horiba LA-960, the appropriate RI to be used for LD-PSA of IMX-104 at the wavelengths used in this analyzer is 1.845 ($n$) 0.01$i$ ($k$). Triplicate analysis of 12 of 25 test samples passed the USP <429> standard for D10, D50, and D90 with CV values less than 15%, 10%, and 15%, respectively (USP 2016). Of the samples that did not pass the CV test, 9 of 13 were found to get finer with successive runs. This phenomenon was potentially caused by physical reduction in particle size that contributed to nonpassing CV values and not an incorrect estimation of RI. The observed sample "fining" during LD-PSA also has implications for measurement precision of rerun, replicate samples. In this case, the most accurate PSD likely results from the first replicate.

The results of the LD-PSA analysis of both LO and partial detonations tend to be bimodal with peaks centering over approximately 500–1000 μm and 50–100 μm. The results of LO-3 agree well with the sieve stack analysis, indicating that the majority of the material by volume is less than 500 μm. The results from LO-6 show high consistency of PSD shape for all samples, no matter the distance from the point of detonation. The most variability with distance from the point of detonation was observed in the data for LO-2, which was also the sample with the highest overall sampled mass.

Although comparisons between PSDs measured through sieve stack and LD-PSA show general agreement, it is clear that LD-PSA results are more highly resolved. LD-PSA also provides a better understanding of size fractions less than 1 mm where the difference between the two methods ranged from 0.1%–21.9%. In addition to this, reduced sample processing and analysis times make LD-PSA a more efficient method and therefore more cost effective when performing investigations with large sample counts. For samples with a range of particle sizes above 2 mm, sieve stack still has a role to play when characterizing large postdetonation particles.

Our investigation brought to light the potential for sample fining during the LD-PSA process and reduction in larger particles causing an increase in CV values for smaller diameters. Variation in particle-size measurements by LD-PSA that do not indicate fining also warrant further investigation into potential causes for such variation. To avoid these situations during RI validation, we recommendation that, whenever possible, the RI of a material be determined through optical measurement or calculated

using optical properties of a material's components. This can then be confirmed through the estimation process used in this study. However, when these options are not available, as was the case in this study, the process described here are reliable and efficient for processing materials with "unknown" properties. By continuing to refine and apply this process for insensitive and conventional energetic compounds, particle characteristics from LO detonations can be directly measured and incorporated into fate and transport models, creating more-accurate range management tools.

# References

Chendorain, M. D., L. D. Steward, and B. Packer. 2005. "Corrosion of Unexploded Ordnance in Soil-Field Results." *Environmental Science and Technology* 30:2442–2447.

Dauphin, L., and C. Doyle. 2000. *Report of Findings for Study of Ammunition Dud and Low-Order Detonation Rates*. McAlester, OK: United States Army Defense Ammunition Center.

Dontsova, K., S. Taylor, R. Pesce-Rodriguez, M. Brusseau, J. Arthur, N. Mark, M. Walsh, J. Lever, and J. Šimůnek. 2014. *Dissolution of NTO, DNAN, and Insensitive Munitions Formulations and Their Fates in Soils*. ERDC/CRREL TR-14-23. Hanover, NH: U.S. Army Engineer Research and Development Center.

Headrick, J. 2015. "Particle Size Image Analysis of Explosive Formulation & Ingredients." In *2015 Insensitive Munitions and Energetic Materials Technology Symposium*, May 2015. https://imemg.org/wp-content/uploads/2015/06/4B5-17289-Particle-Size-Image-Analysis-of-Explosive-Formulation-Ingredients.pdf.

Hewitt, A. D., T. F. Jenkins, M. E. Walsh, M. R. Walsh, and S. Taylor. 2005. "RDX and TNT Residues from Live-Fire and Blow-in-Place Detonations." *Chemosphere* 61:888–894.

Horiba. 2005. *Method Development for Wide Size-Distribution Samples*. AN145. Irvine, CA: Horiba Instruments, Inc. https://www.horiba.com/fileadmin/uploads/Scientific/Documents/PSA/AN145_app.pdf.

Horiba. 2014. *Method Expert: Guided, Automated Method Development for the LA-950/960*. WP001. Irvine, CA: Horiba Instruments, Inc. https://www.horiba.com/fileadmin/uploads/Scientific/Documents/PSA/WP001.pdf.

Horiba. 2008a. *Refractive Index Selection for Powder Mixtures*. AN157. Irvine, CA: Horiba Instruments, Inc. https://www.horiba.com/fileadmin/uploads/Scientific/Documents/PSA/AN157_app.pdf.

Horiba. 2008b. *Understanding the Chi Square and R Parameter Calculations in the LA-950 Software*. TN153. Irvine, CA: Horiba Instruments, Inc. https://www.horiba.com/fileadmin/uploads/Scientific/Documents/PSA/TN153.pdf.

Jenkins, T. F., M. E. Walsh, P. H. Miyares, A. D. Hewitt, N. H. Collins, and T. A. Ranney. 2002. "Use of Snow-Covered Ranges to Estimate Explosives Residues from High-order Detonations of Army Munitions." *Thermochimica Acta* 384:173–185.

Palka, N., and M. Szala. 2016. "Transmission and Reflection Terahertz Spectroscopy of Insensitive Melt-Cast High-Explosive Materials." *Journal of Infrared Milli Terahertz Waves* 37:977–992.

Pennington, J. C., T. F. Jenkins, G. Ampleman, S. Thiboutot, J. M. Brannon, A. D. Hewitt, J. Lewis, S. Brochu, E. Diaz, M. R. Walsh, M. E. Walsh, S. Taylor, J. C. Lynch, J. L. Clausen, T. A. Ranney, C. A. Ramsey, C. A. Hayes, C. L. Grant, M. Charles, S. R. Bigl, S. L. Yost, and K. M. Dontsova. 2006. *Distribution and Fate of Energetics on DoD Test and Training Ranges: Final Report*. ERDC TR-06-13. Vicksburg, MS: U.S. Army Engineer Research and Development Center. http://hdl.handle.net/11681/8521.

Taylor, S., K. Dontsova, M. E. Walsh, and M. R Walsh. 2015. "Outdoor Dissolution of Detonation Residues of Three Insensitive Munitions (IM) formulations." *Chemosphere* 134:250–256.

Taylor, S., A. Hewitt, J. Lever, C. Hayes, L. Perovich, P. Thorne, and C. Daghlian. 2004. "TNT Particle Size Distributions from Detonated 155-mm Howitzer Rounds." *Chemosphere* 55:357–367.

Taylor, S., J. Lever, E. Campbell, L. Perovich, and J. Pennington. 2006. "Characteristics of Composition B Particles from Blow-in-Place Detonations." *Chemosphere* 65:1405–1413.

USP. 2016. "<429> Light Diffraction Measurement of Particle Size." In *35(3) Harmonization Stage 6*. https://www.usp.org/sites/default/files/usp/document/harmonization/gen-chapter/g13_pf_35_3_2009.pdf.

Walsh, M. E., C. M. Collins, M. R. Walsh, C. A. Ramsey, S. Taylor, S. R. Bigl, R. N. Bailey, A. D. Hewitt, and M. Prieksat. 2008. "Energetic Residues and Crater Geometries from the Firing of 120-mm High-Explosive Mortar Projectiles into Eagle River Flats, June 2007." ERDC/CRREL TR-08-10. Hanover, NH: U.S. Army Engineer Research and Development Center.

Walsh, M. R., M. F. Bigl, M. E. Walsh, E. T. Wrobel, S. A. Beal, and T. Temple. 2018. "Physical Simulation of Live-fire Detonations Using Command-Detonation Fuzing." *Propellants, Explosives, Pyrotechnics*, 43 (6): 602–608.

Walsh, M. R., S. Thiboutot, and B. Gullette. 2017. *Characterization of Residues from the Detonation of Insensitive Munitions*. SERDP Project ER-2219. Alexandria, VA: SERDP. https://www.serdp-estcp.org/content/download/47274/451031/file/ER-2219%20Final%20Report.pdf.

Walsh, M. R., S. Thiboutot, M. E. Walsh, G. Ampleman, R. Martel, I. Poulin, and S. Taylor. 2011. *Characterization and Fate of Gun and Rocket Propellant Residues on Testing and Training Ranges: Final Report*. ERDC/CRREL TR-11-13. Hanover, NH: U.S. Army Engineer Research and Development Center. http://hdl.handle.net/11681/5515.

Walsh, M. R., M. E. Walsh, and J. W. Hug. 2011. "A Simple Device for Initiating High Order Detonations." Chapter 6 in *Characterization and Fate of Gun and Rocket Propellant Residues on Testing and Training Ranges: Final Report*. ERDC/CRREL TR-11-13. Hanover, NH: U.S. Army Engineer Research and Development Center.

Walsh, M. R., M. E. Walsh, I. Poulin, S. Taylor, and T. A. Douglas. 2011. "Energetic Residues from the Detonation of Common US Ordnance." *International Journal of Energetic Materials and Chemical Propulsion* 10 (2): 169–186.

Walsh, M. R., M. E. Walsh, C. A. Ramsey, S. Brochu, S. Thiboutot, and G. Ampleman. 2013. "Perchlorate Contamination from the Detonation of Insensitive High-Explosive Rounds." *Journal of Hazardous Material* 262:228–233.

Walsh, M. R., M. E. Walsh, C. A. Ramsey, S. Taylor, D. Ringelberg, J. Zufelt, S. Thiboutot, G. Ampleman, and E. Diaz. 2013. "Characterization of PAX-21 Insensitive Munition Detonation Residues." *Propellants, Explosives, Pyrotechnics* 38:399–409.

# Appendix A: PSDs That Did Not Pass CV Test

Note the increase in the percent by volume for the lower particle sizes with each successive run, a potential indicator of the diminution of the particles through the multiple-measurement process.

Figure A-1. Full set of PSD plots of LO particle samples that did not pass the CV test.

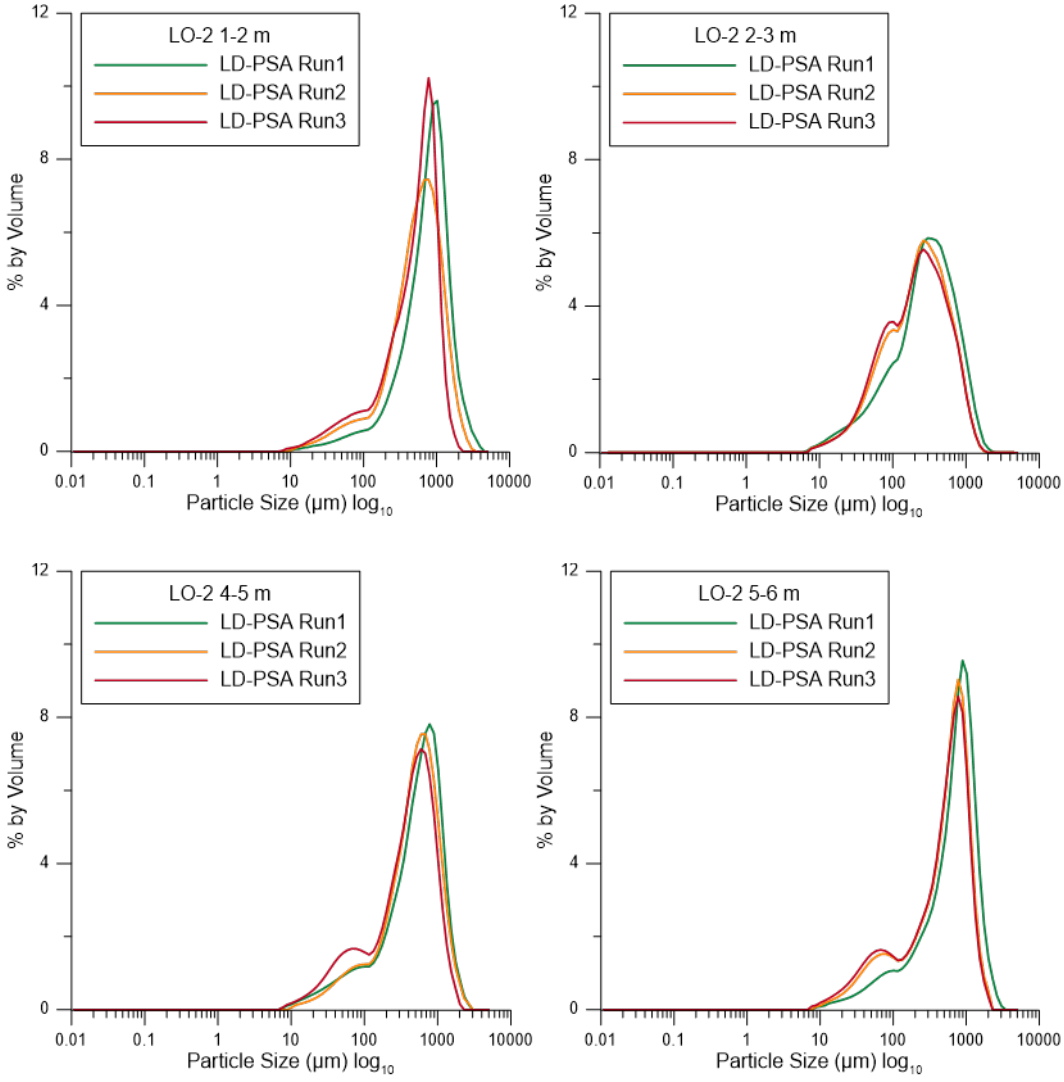

Figure A-1 (cont.). Full set of PSD plots of LO particle samples that did not pass the CV test.

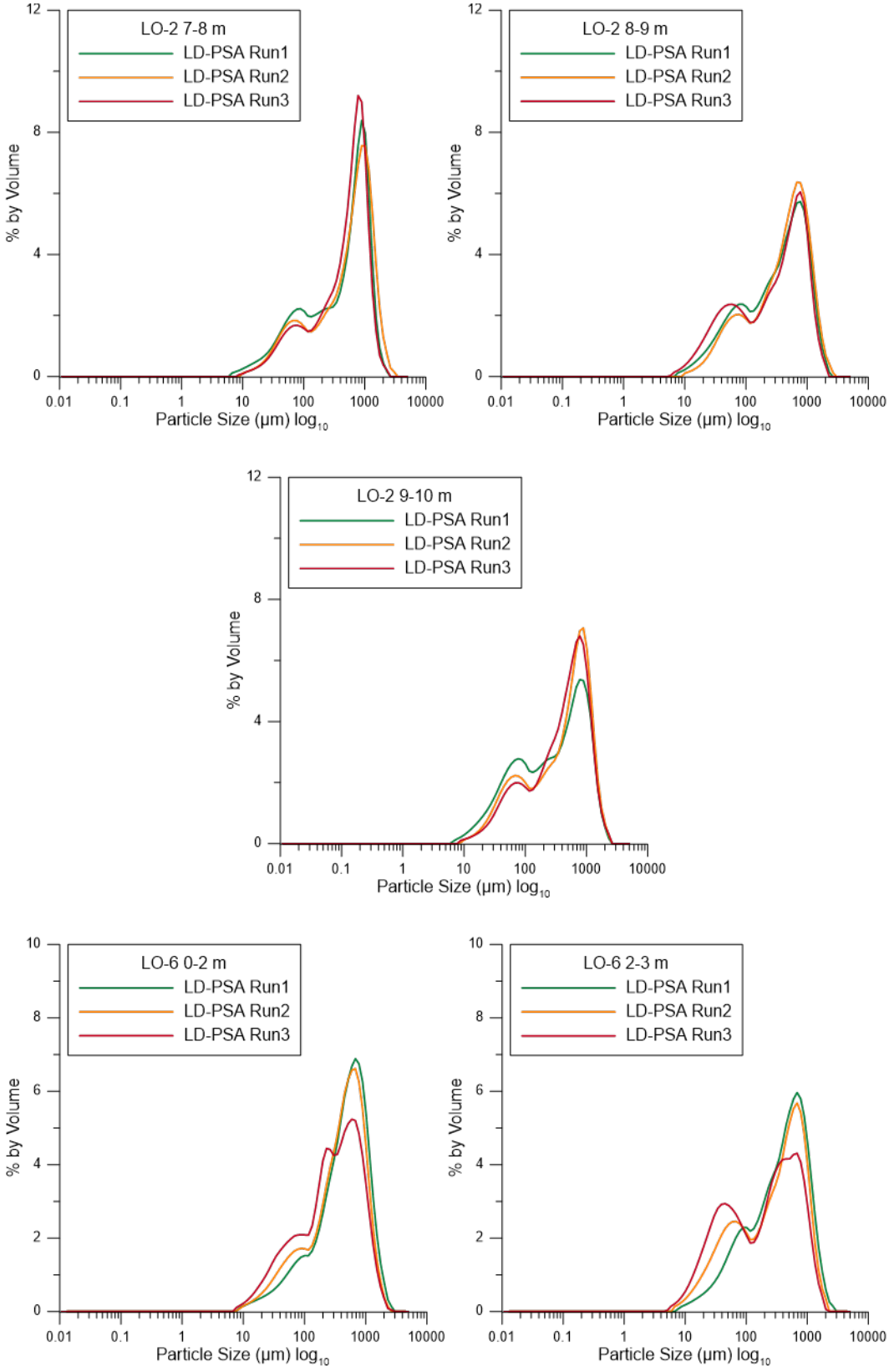

Figure A-1 (cont.). Full set of PSD plots of LO particle samples that did not pass the CV test.

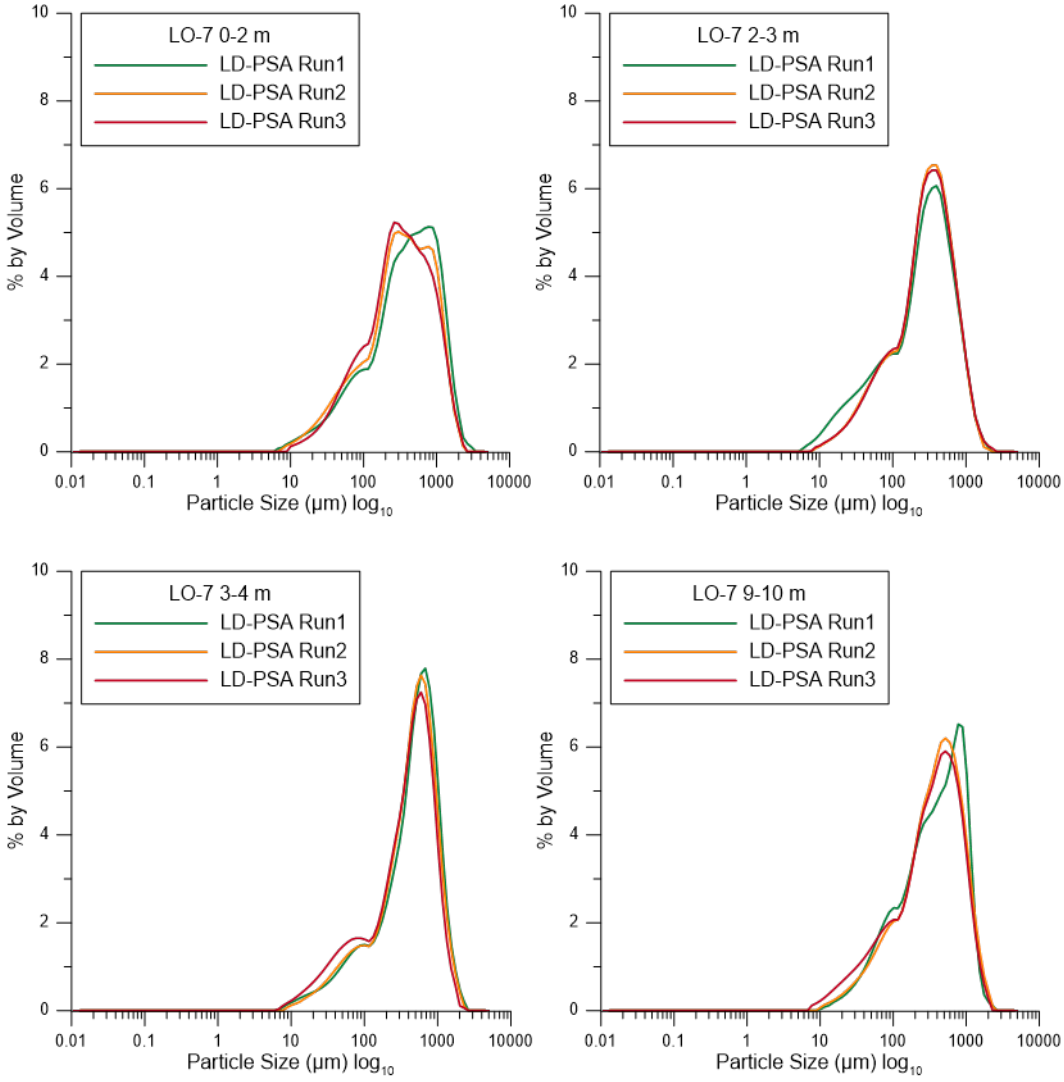

Figure A-2. Summary of D10, D50, D90, and mean particle size for all samples that did not pass the CV standard.

| Sample ID | D10 (µm) | D50 (µm) | D90 (µm) | Mean (µm) |
|---|---|---|---|---|
| L0-2 1–2 m Run1 | 237.9 | 754.8 | 1456.8 | 815.9 |
| L0-2 1–2 m Run2 | 131.7 | 538.5 | 1199.1 | 620.3 |
| L0-2 1–2 m Run3 | 176.4 | 497.2 | 928.5 | 533.6 |
| L0-2 2–3 m Run1 | 53.0 | 273.1 | 765.7 | 352.1 |
| L0-2 2–3 m Run2 | 49.4 | 220.1 | 638.6 | 288.5 |
| L0-2 2–3 m Run3 | 46.8 | 208.0 | 636.6 | 280.8 |
| L0-2 4–5 m Run1 | 116.0 | 513.4 | 1089.2 | 572.4 |
| L0-2 4–5 m Run2 | 106.7 | 469.8 | 1034.3 | 536.2 |
| L0-2 4–5 m Run3 | 52.2 | 391.5 | 897.1 | 443.7 |
| L0-2 5–6 m Run1 | 138.2 | 646.3 | 1305.4 | 703.3 |
| L0-2 5–6 m Run2 | 67.3 | 513.2 | 1036.2 | 544.3 |
| L0-2 5–6 m Run3 | 52.1 | 486.6 | 1004.4 | 517.3 |
| L0-2 7–8 m Run1 | 48.0 | 493.8 | 1086.7 | 530.0 |
| L0-2 7–8 m Run2 | 55.2 | 570.5 | 1280.8 | 625.9 |
| L0-2 7–8 m Run3 | 37.8 | 335.3 | 798.4 | 380.3 |
| L0-2 8–9 m Run1 | 41.7 | 350.6 | 1006.7 | 448.6 |
| L0-2 8–9 m Run2 | 51.4 | 424.2 | 1074.5 | 504.1 |
| L0-2 8–9 m Run3 | 29.9 | 319.4 | 949.6 | 415.0 |
| L0-2 9–10 m Run1 | 36.3 | 305.8 | 1034.4 | 437.9 |
| L0-2 9–10 m Run2 | 46.2 | 447.0 | 1093.9 | 514.4 |
| L0-2 9–10 m Run3 | 49.5 | 480.9 | 1137.7 | 543.3 |
| L0-6 0–2 m Run1 | 80.4 | 463.3 | 1061.9 | 530.7 |
| L0-6 0–2 m Run2 | 59.7 | 395.9 | 954.2 | 464.2 |
| L0-6 0–2 m Run3 | 45.6 | 326.3 | 836.9 | 394.0 |
| L0-6 2–3 m Run1 | 55.3 | 386.7 | 1003.6 | 468.4 |
| L0-6 2–3 m Run2 | 32.2 | 302.9 | 911.0 | 397.3 |
| L0-6 2–3 m Run3 | 23.2 | 216.8 | 771.6 | 318.5 |
| L0-7 0–2 m Run1 | 65.0 | 394.5 | 1070.2 | 495.9 |
| L0-7 0–2 m Run2 | 51.5 | 313.4 | 978.1 | 430.7 |
| L0-7 0–2 m Run3 | 59.1 | 295.0 | 961.5 | 417.6 |
| L0-7 2–3 m Run1 | 35.5 | 265.1 | 690.5 | 322.9 |
| L0-7 2–3 m Run2 | 58.3 | 276.5 | 696.7 | 336.7 |
| L0-7 2–3 m Run3 | 65.2 | 285.6 | 696.0 | 341.9 |
| L0-7 3–4 m Run1 | 77.7 | 458.3 | 981.0 | 507.7 |
| L0-7 3–4 m Run2 | 84.6 | 423.7 | 953.4 | 482.9 |
| L0-7 3–4 m Run3 | 50.8 | 381.6 | 874.9 | 431.9 |
| L0-7 9–10 m Run1 | 77.5 | 406.3 | 867.4 | 449.0 |
| L0-7 9–10 m Run2 | 69.7 | 354.9 | 937.4 | 442.8 |
| L0-7 9–10 m Run3 | 49.5 | 324.5 | 884.0 | 408.2 |

# Appendix B: PSDs That Passes the Triplicate Analyses CV Standard for D10, D50, and D90

Note the high degree of overlap between successive runs, indicating good repeatability for this analysis and RI kernel.

Figure B-1. Full set of PSD plots of LO particle samples that passed the CV test.

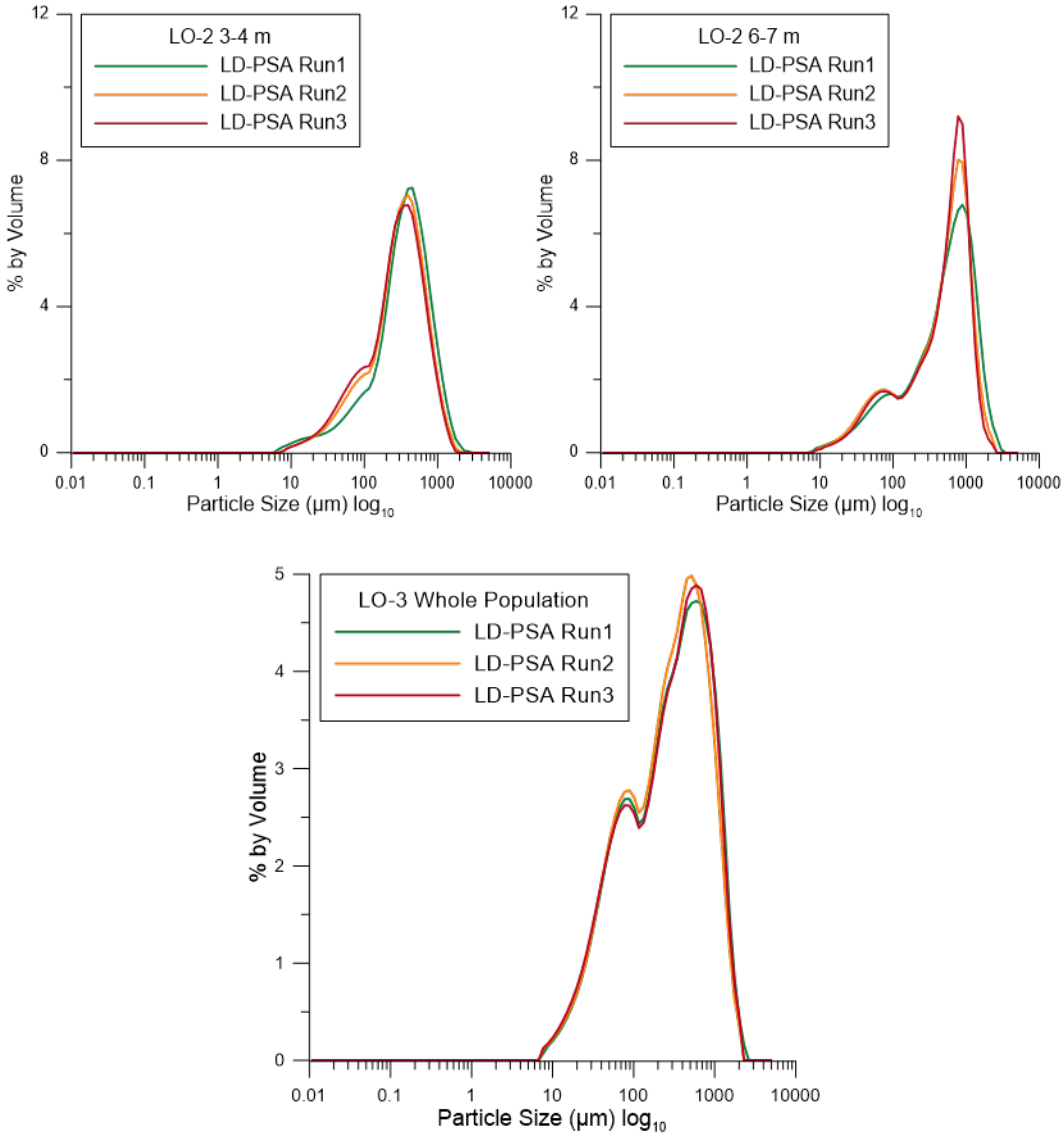

Figure B-1 (cont.). Full set of PSD plots of LO particle samples that passed the CV test.

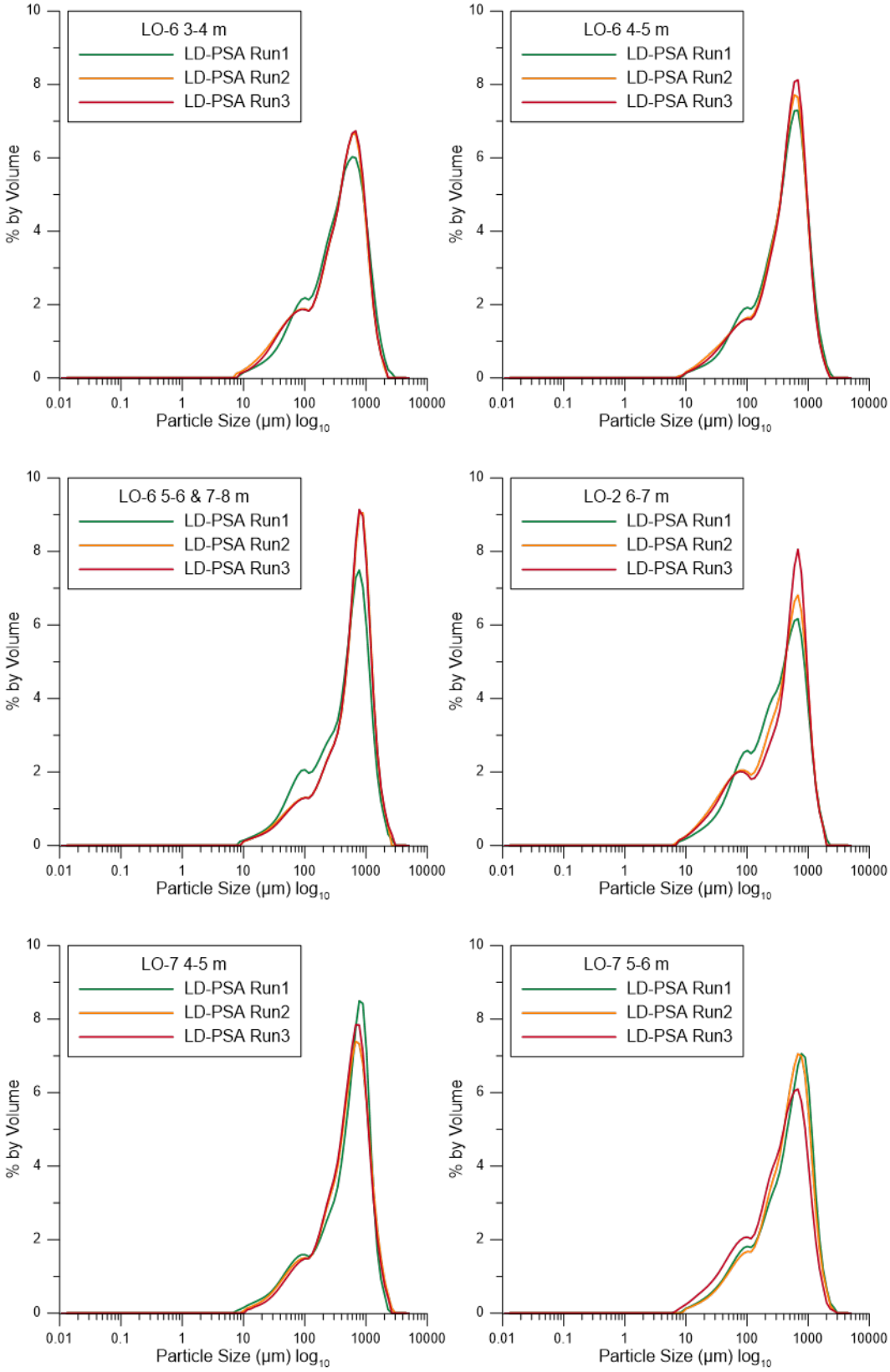

Figure B-1 (cont.). Full set of PSD plots of LO particle samples that passed the CV test.

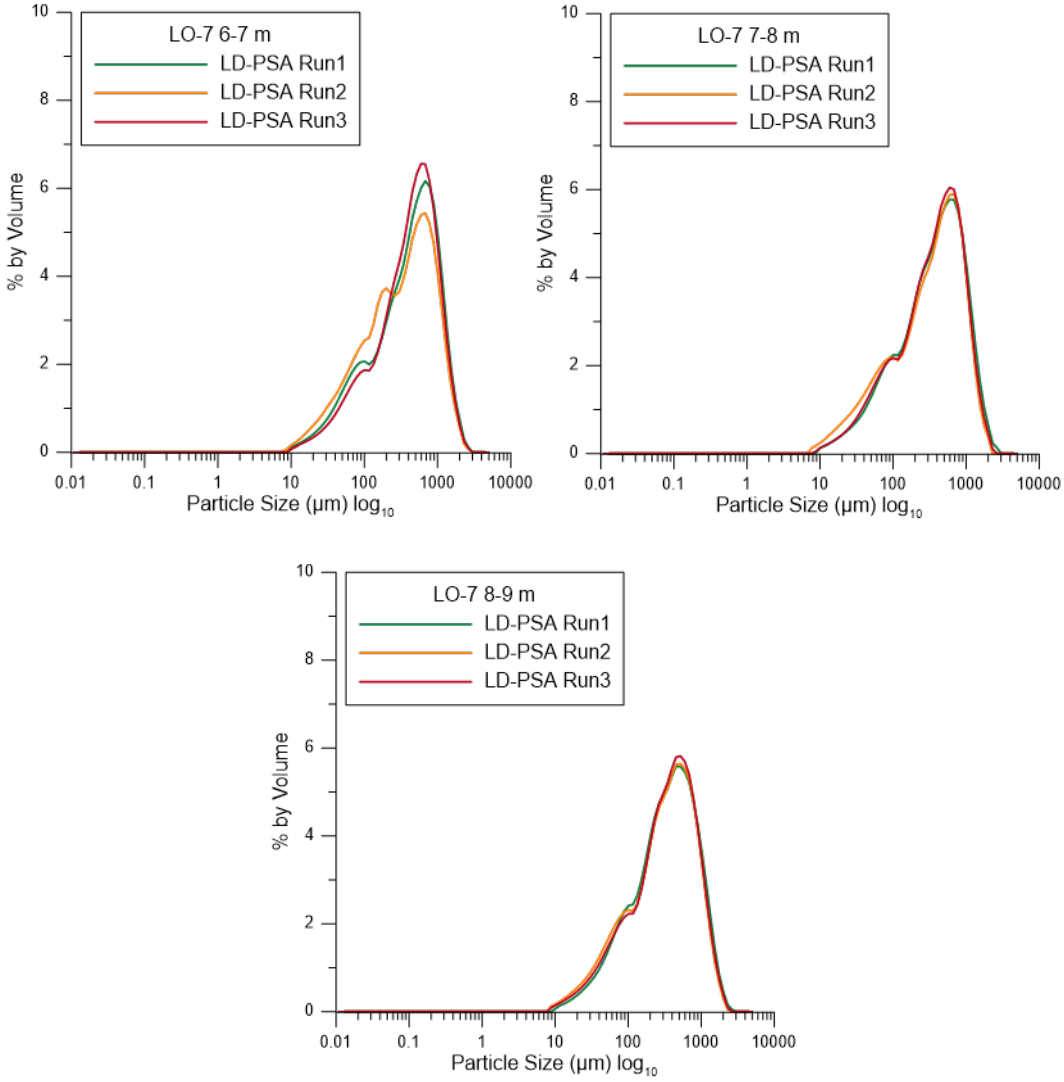

# Appendix C: LD-PSA and Sieve Stack Comparison Plots for All Samples

Figure C-1. Cumulative percent by mass of sieve stack data overlain by cumulative percent by volume curves from LD-PSA for all samples analyzed.

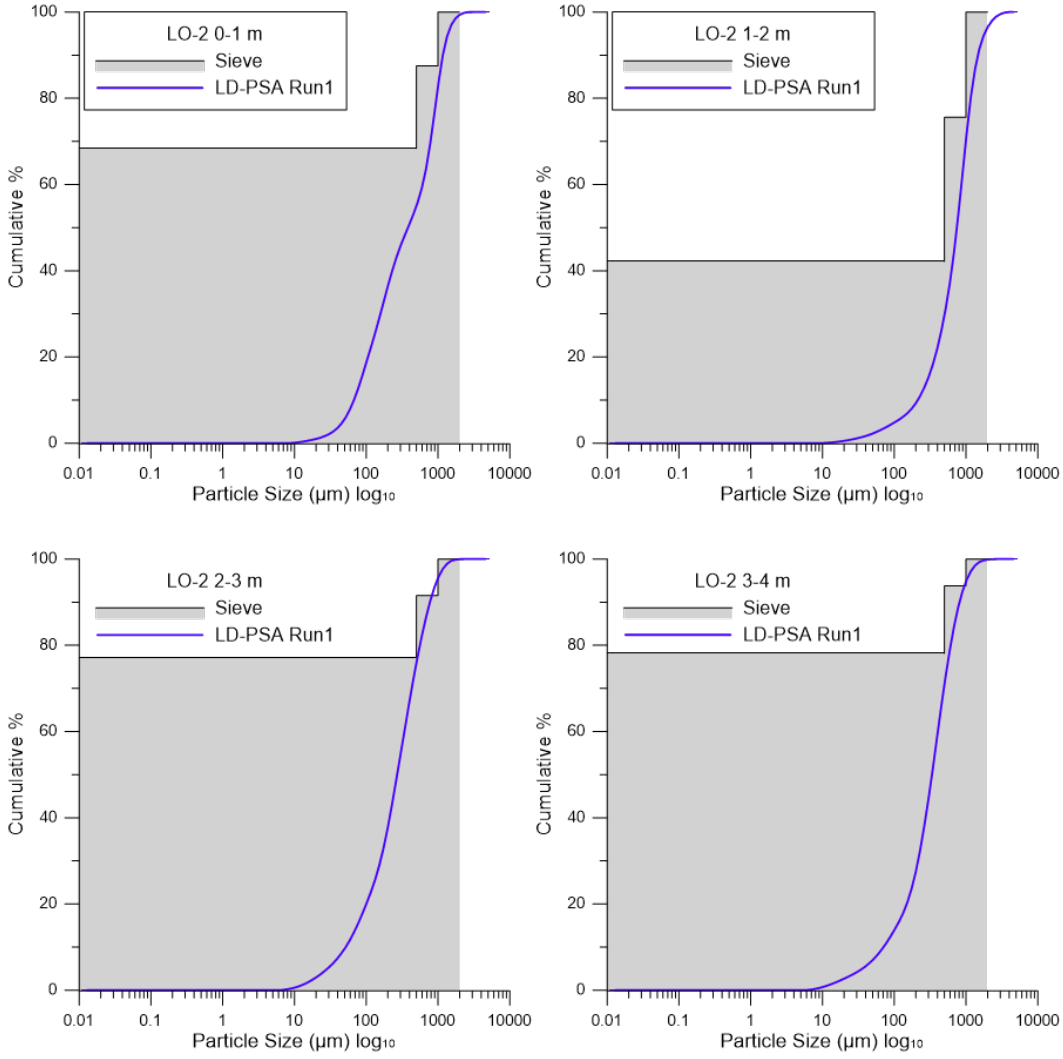

Figure C-1 (cont.). Cumulative percent by mass of sieve stack data overlain by cumulative percent by volume curves from LD-PSA for all samples analyzed.

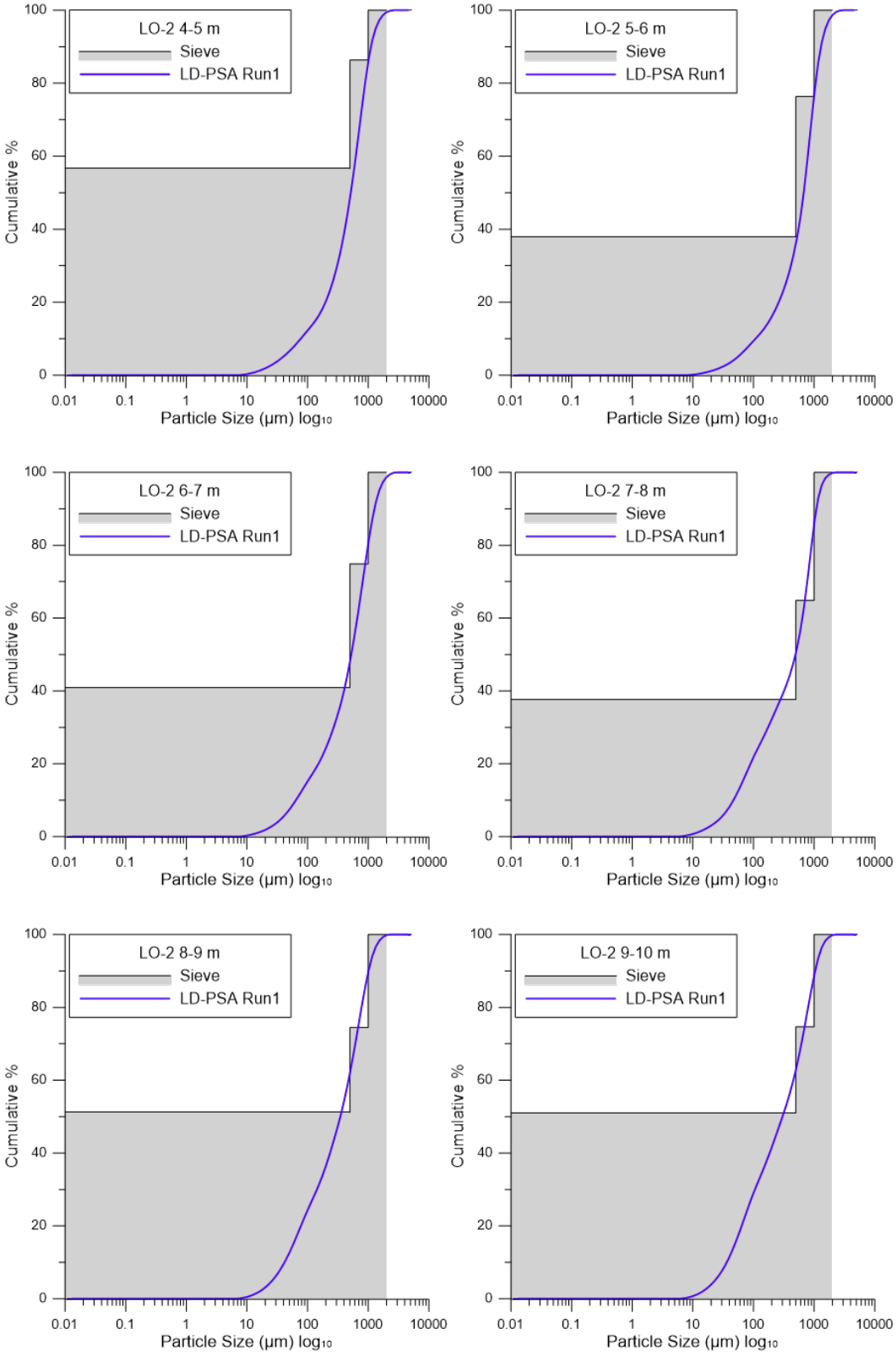

Figure C-1 (cont.). Cumulative percent by mass of sieve stack data overlain by cumulative percent by volume curves from LD-PSA for all samples analyzed.

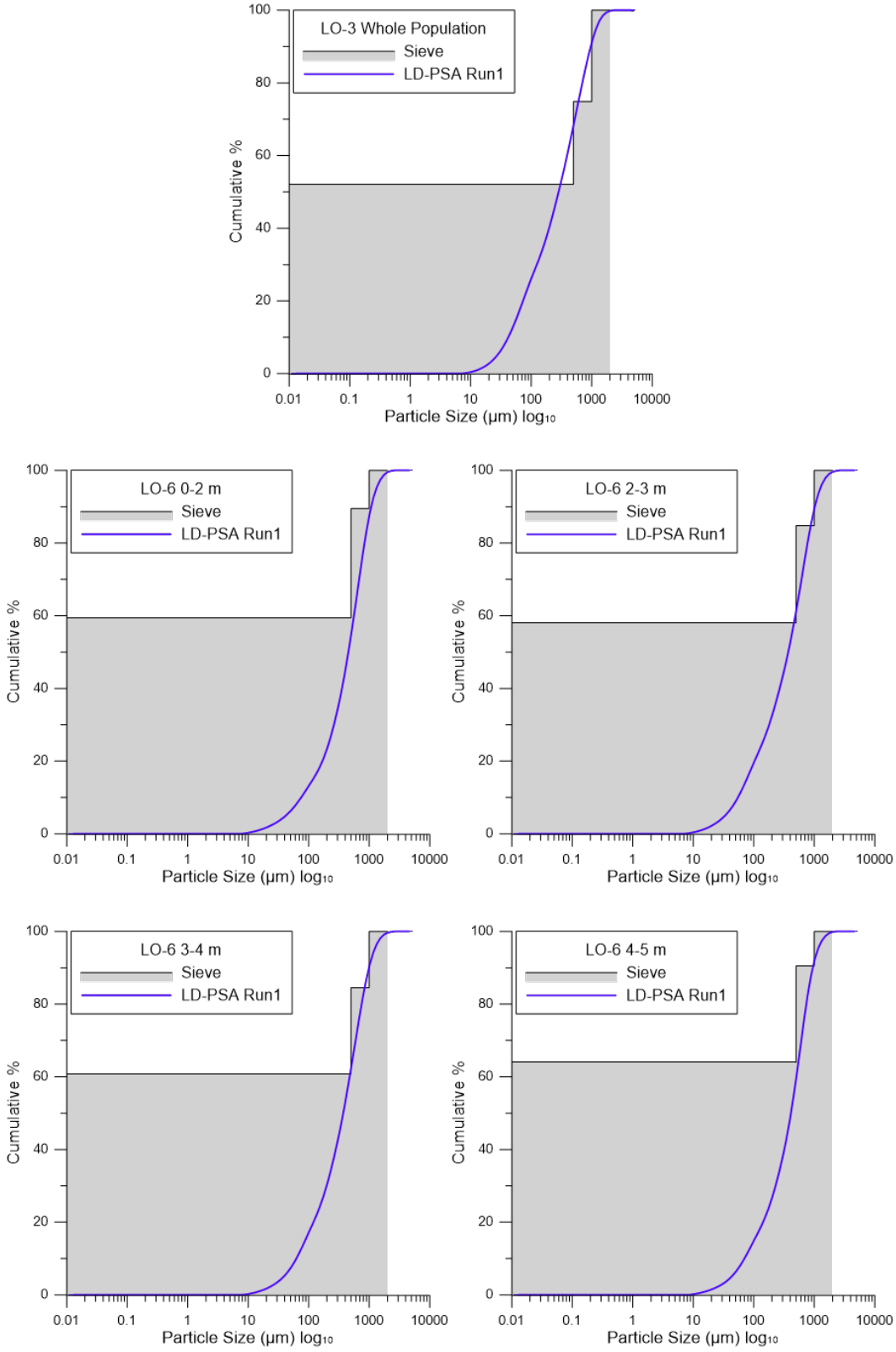

Figure C-1 (cont.). Cumulative percent by mass of sieve stack data overlain by cumulative percent by volume curves from LD-PSA for all samples analyzed.

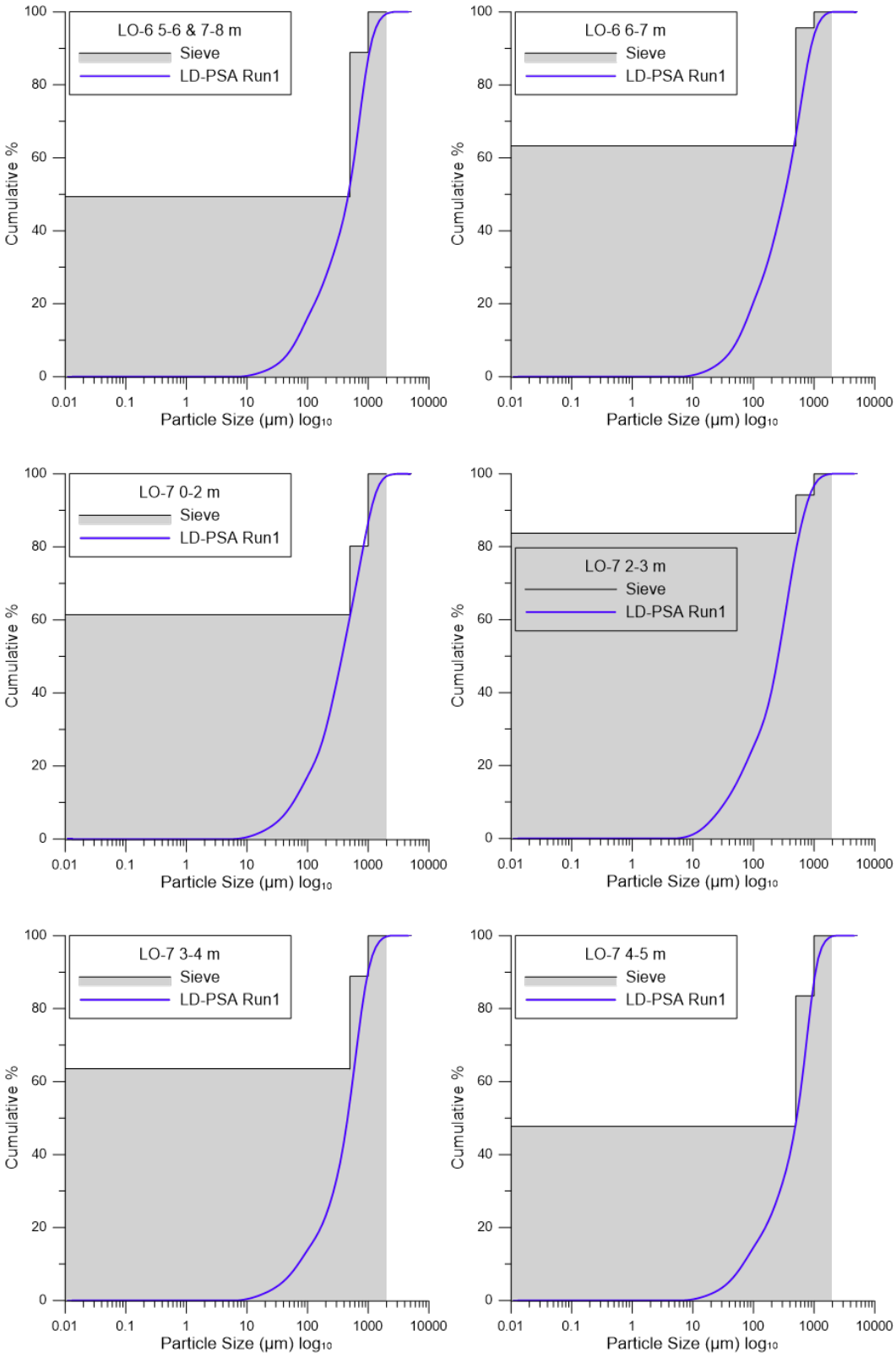

Figure C-1 (cont.). Cumulative percent by mass of sieve stack data overlain by cumulative percent by volume curves from LD-PSA for all samples analyzed.

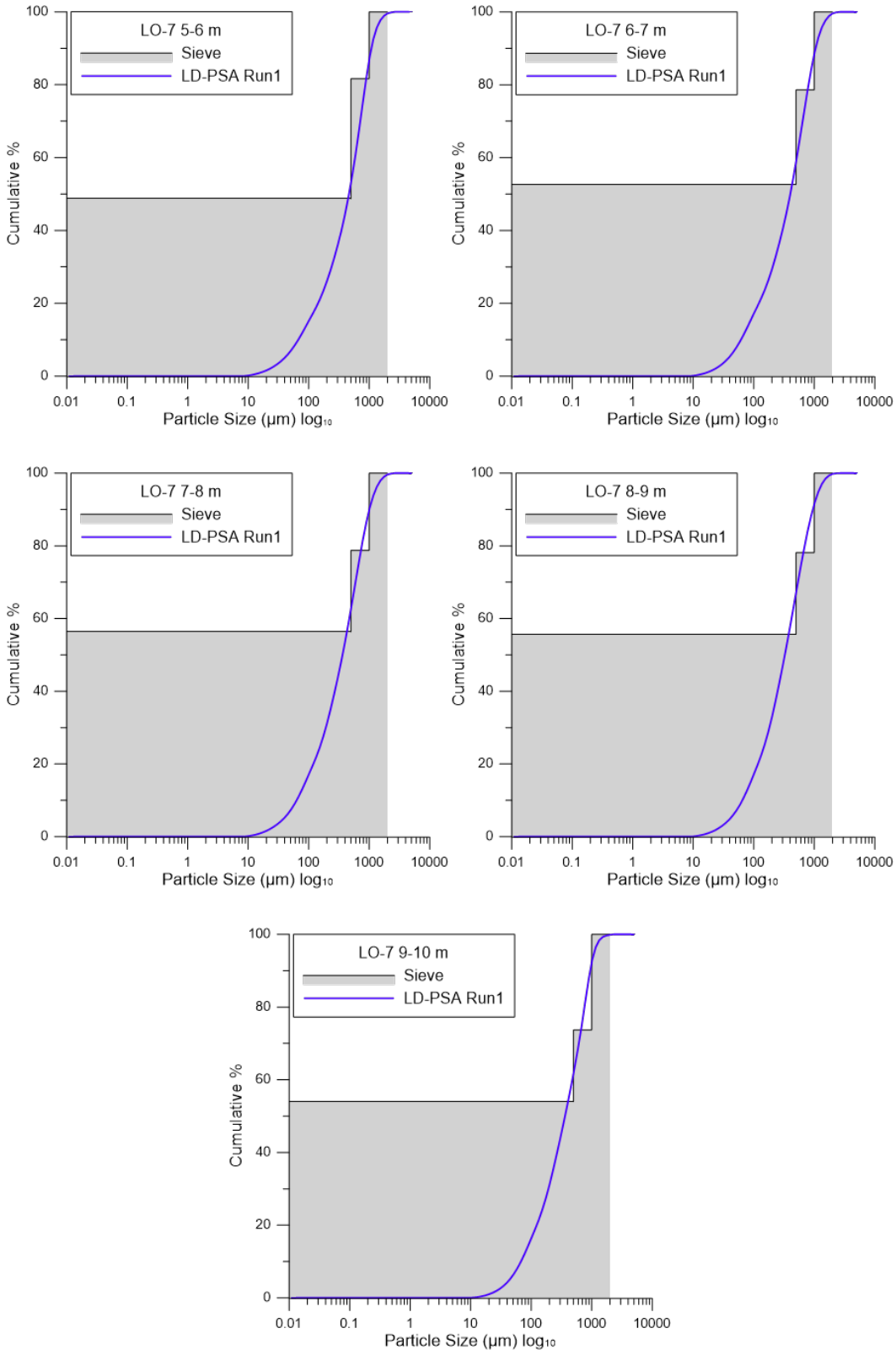

# Appendix D: PSD Plots for All Samples Sieved <2 mm

Figure D-1. Particle size distributions for Run 1 of all samples analyzed.

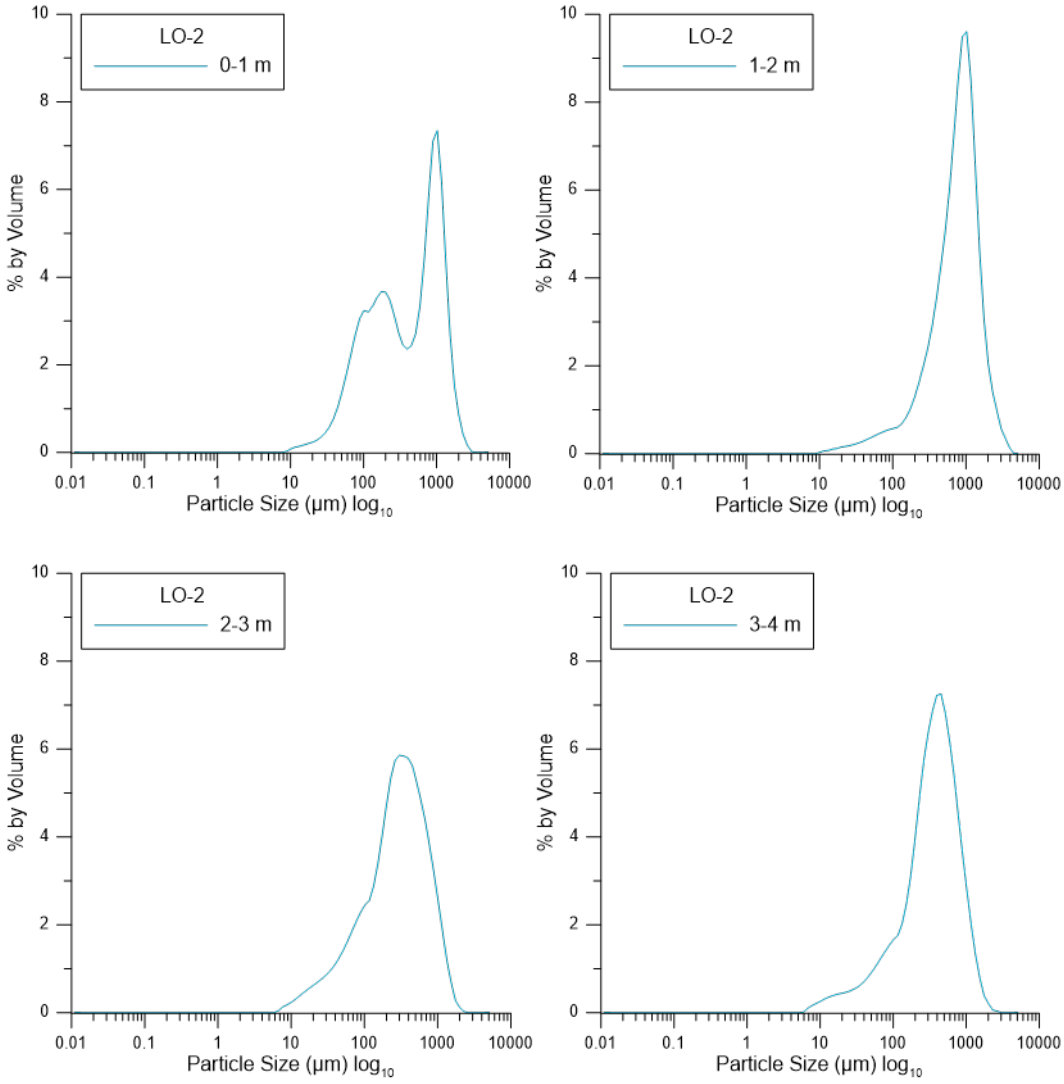

Figure D-1 (cont.). Particle size distributions for Run 1 of all samples analyzed.

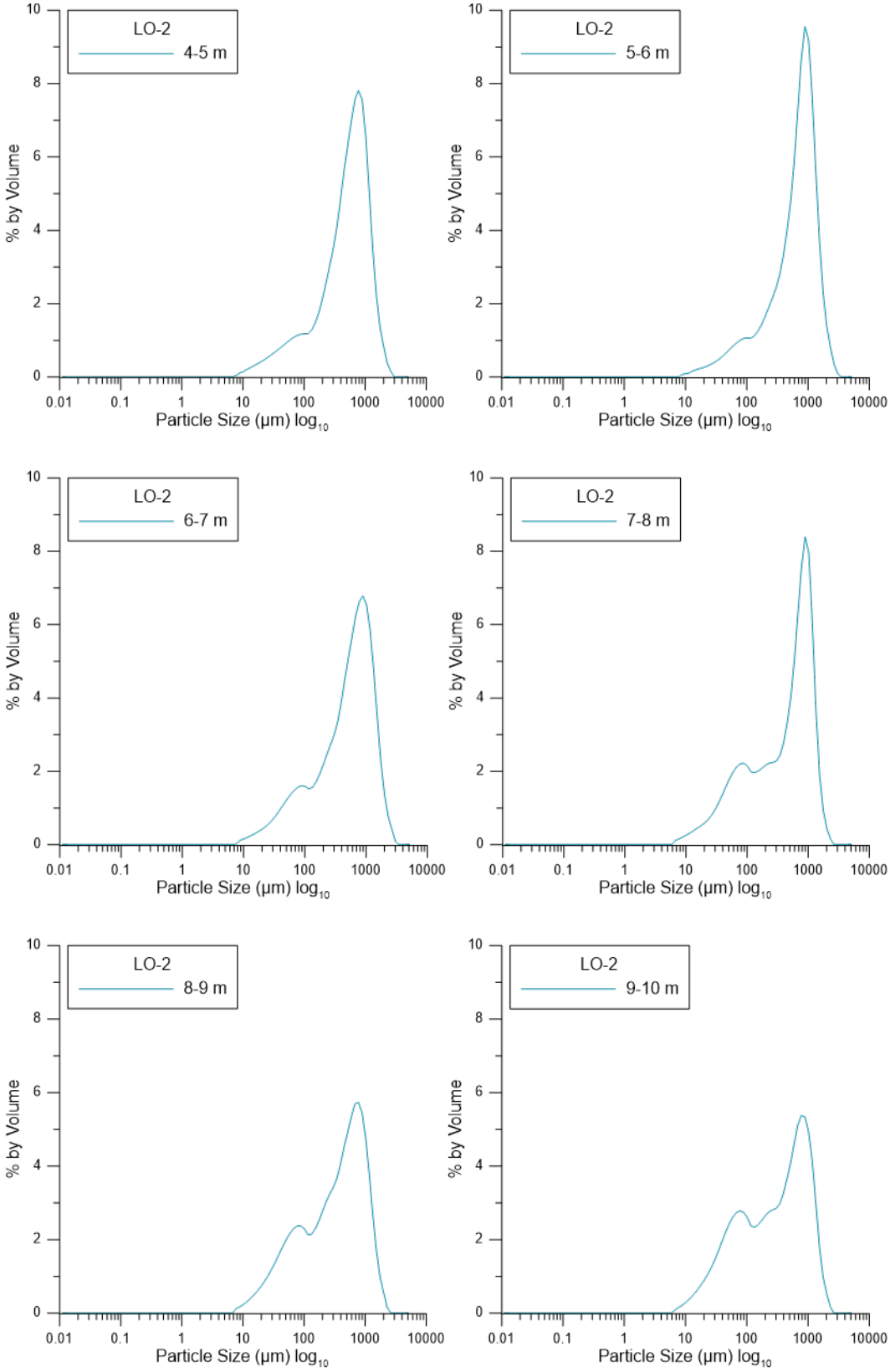

Figure D-1 (cont.). Particle size distributions for Run 1 of all samples analyzed.

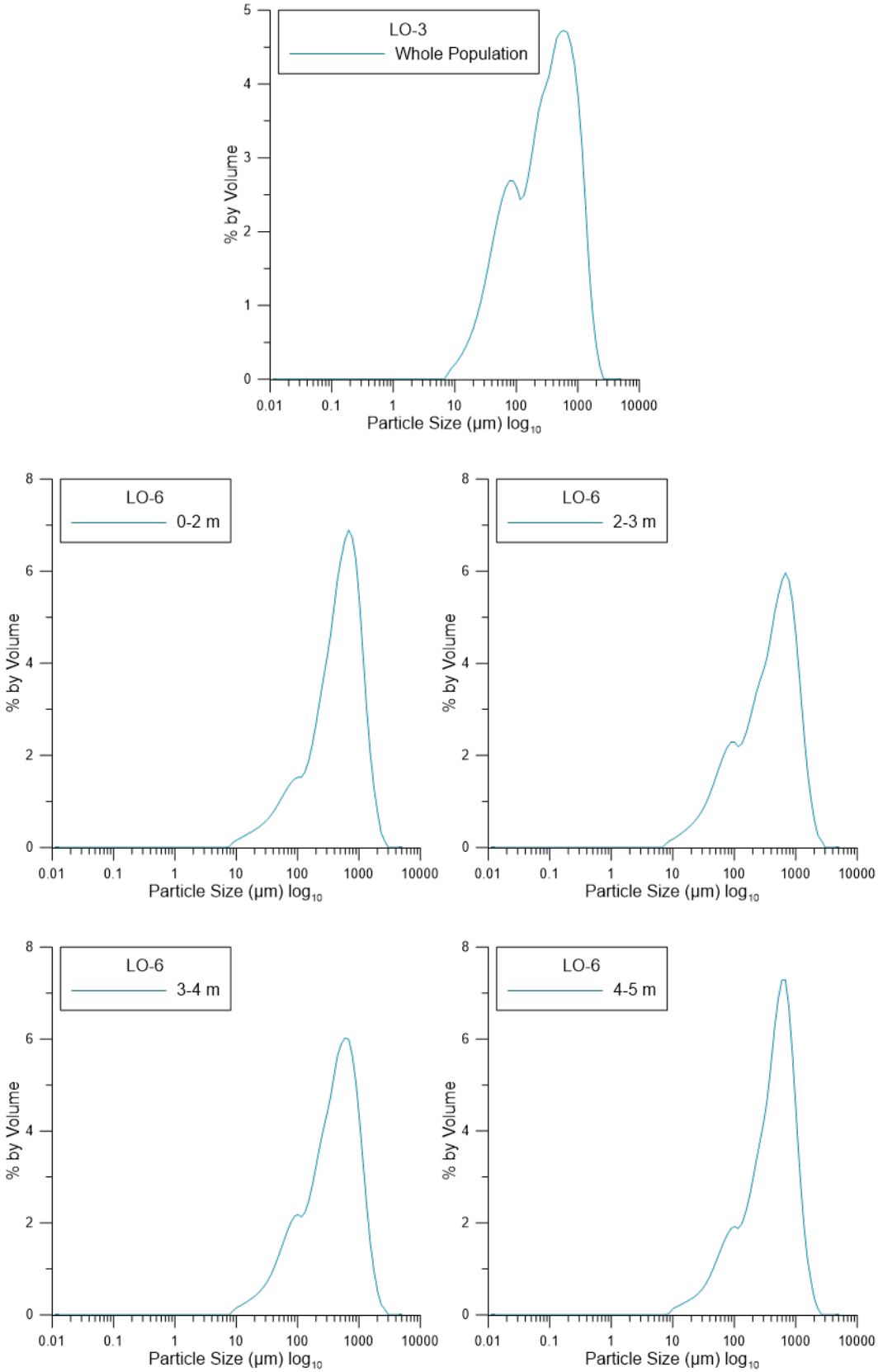

Figure D-1 (cont.). Particle size distributions for Run 1 of all samples analyzed.

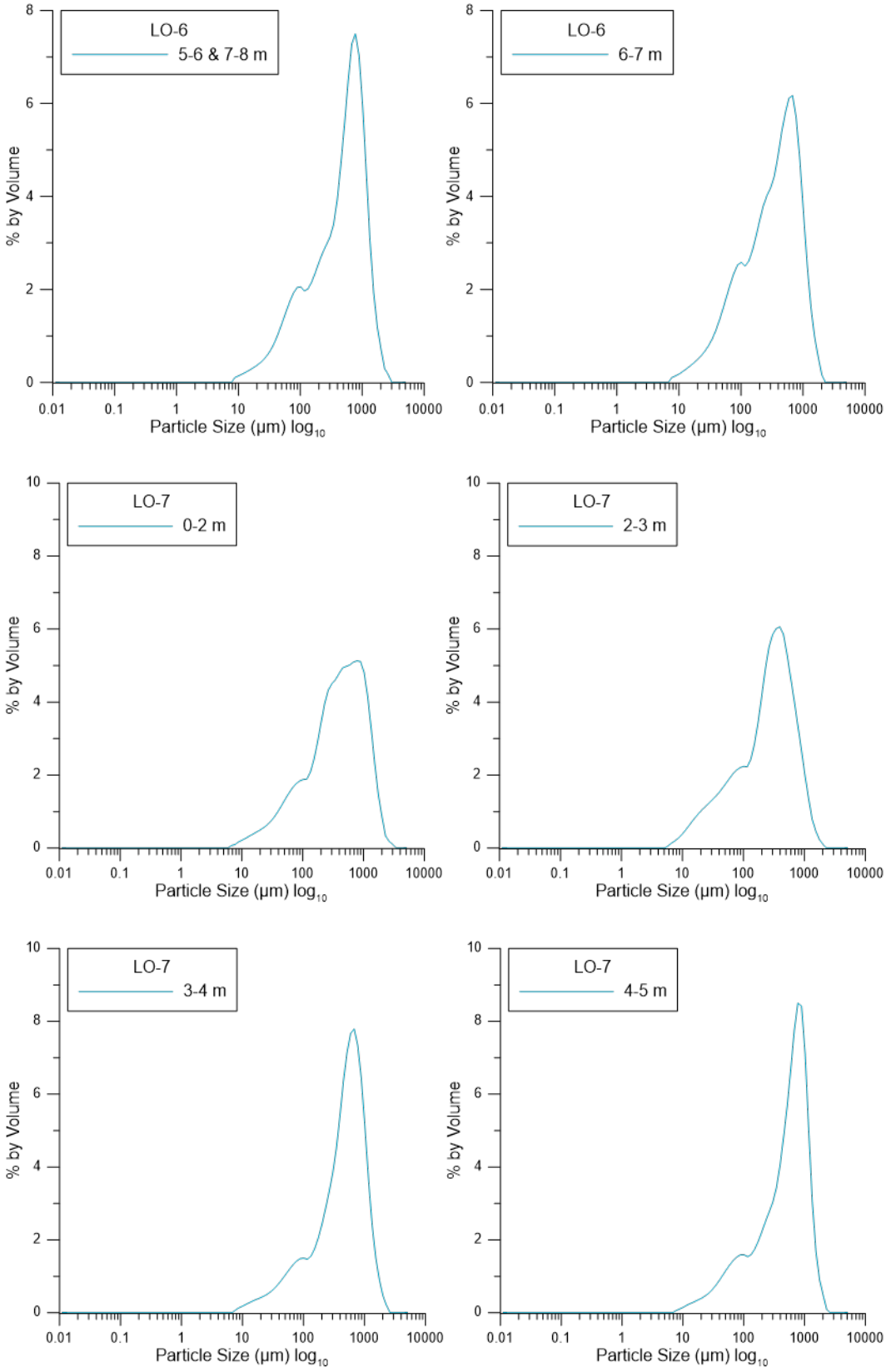

Figure D-1 (cont.). Particle size distributions for Run 1 of all samples analyzed.

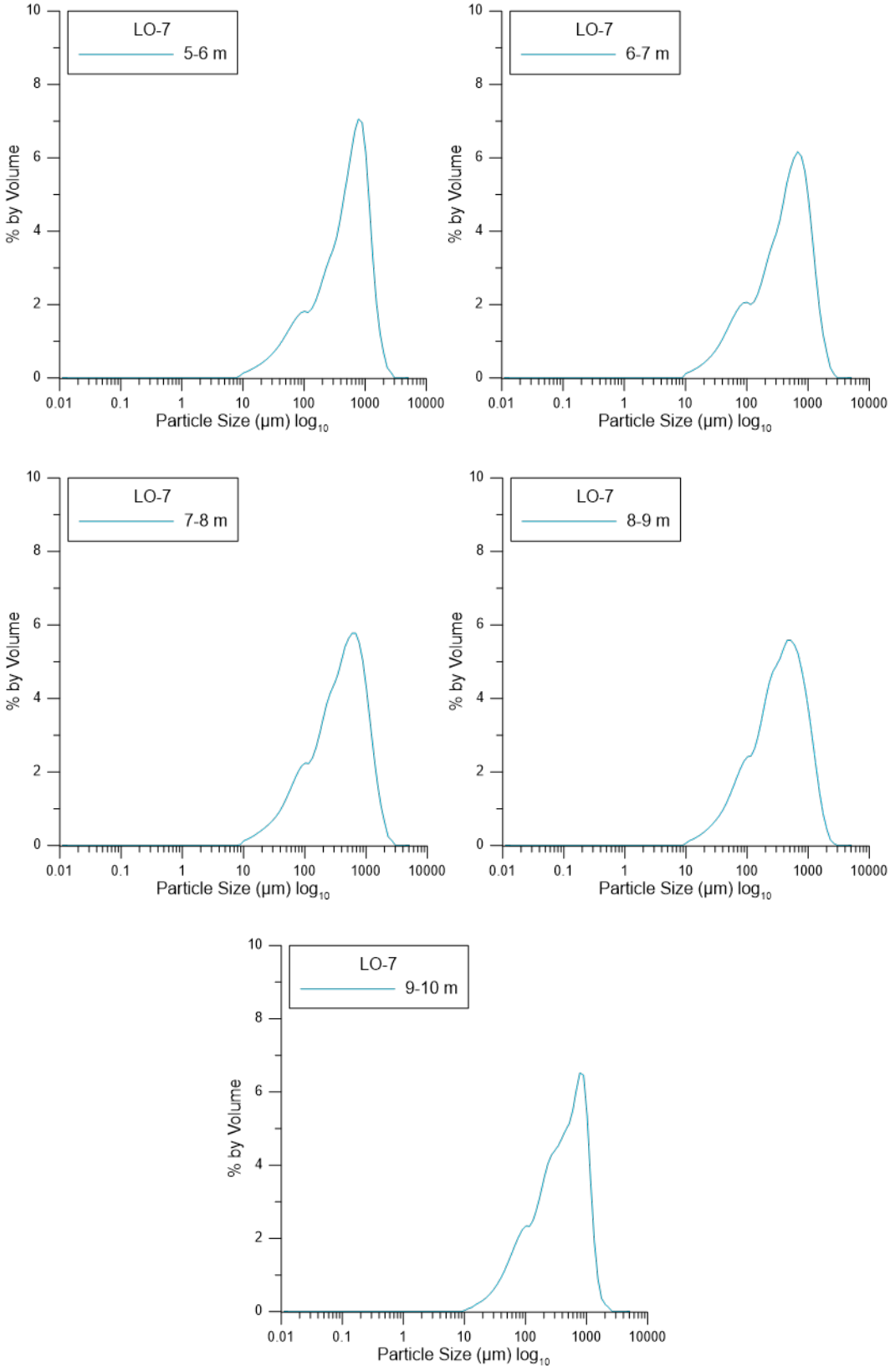

# Appendix E: Cumulative Percent Data

Table E-1. Cumulative percent data from sieve stack and LD-PSA analysis of the same sample. LD-PSA data has been down selected by sieve bin size for direct comparison.

| Sample ID | <0.5 mm | 0.5–1 mm | 1–2 mm |
|---|---|---|---|
| LO-2 0–1 m—Sieve | 68.3 | 87.5 | 100.0 |
| LO-2 0–1 m—LD-PSA | 55.7 | 83.8 | 99.4 |
| *Difference* | *12.6* | *3.7* | *0.6* |
| LO-2 1–2 m—Sieve | 42.1 | 75.6 | 100.0 |
| LO-2 1–2 m—LD-PSA | 31.0 | 71.8 | 96.6 |
| *Difference* | *11.1* | *3.8* | *3.4* |
| LO-2 2–3 m—Sieve | 77.1 | 91.5 | 100.0 |
| LO-2 2–3 m—LD-PSA | 77.2 | 95.9 | 100.0 |
| *Difference* | *0.1* | *4.4* | *0.0* |
| LO-2 3–4 m—Sieve | 78.1 | 93.8 | 100.0 |
| LO-2 3–4 m—LD-PSA | 72.7 | 95.2 | 99.9 |
| *Difference* | *5.4* | *1.4* | *0.1* |
| LO-2 4–5 m—Sieve | 56.6 | 86.3 | 100.0 |
| LO-2 4–5 m—LD-PSA | 50.2 | 86.7 | 99.5 |
| *Difference* | *6.4* | *0.4* | *0.5* |
| LO-2 5–6 m—Sieve | 38.0 | 76.3 | 100.0 |
| LO-2 5–6 m—LD-PSA | 37.3 | 77.9 | 98.7 |
| *Difference* | *0.6* | *1.5* | *1.3* |
| LO-2 6–7 m—Sieve | 41.0 | 74.9 | 100.0 |
| LO-2 6–7 m—LD-PSA | 49.3 | 81.2 | 98.7 |
| *Difference* | *8.3* | *6.4* | *1.3* |
| LO-2 7–8 m—Sieve | 37.8 | 64.8 | 100.0 |
| LO-2 7–8 m—LD-PSA | 51.5 | 86.8 | 99.8 |
| *Difference* | *13.7* | *21.9* | *0.2* |
| LO-2 8–9 m—Sieve | 51.1 | 74.5 | 100.0 |
| LO-2 8–9 m—LD-PSA | 63.3 | 90.3 | 99.9 |
| *Difference* | *12.2* | *15.8* | *0.1* |
| LO-2 9–10 m—Sieve | 51.1 | 74.7 | 100.0 |
| LO-2 9–10 m—LD-PSA | 63.9 | 89.3 | 99.8 |
| *Difference* | *12.9* | *14.6* | *0.2* |
| LO-3 Whole Population—Sieve | 52.2 | 74.8 | 100.0 |
| LO-3 Whole Population—LD-PSA | 69.6 | 91.6 | 99.8 |
| *Difference* | *17.4* | *16.7* | *0.2* |
| LO-6 0–2 m—Sieve | 59.5 | 89.5 | 100.0 |
| LO-6 0–2 m—LD-PSA | 56.2 | 88.2 | 99.5 |

| Sample ID | <0.5 mm | 0.5–1 mm | 1–2 mm |
|---|---|---|---|
| *Difference* | *3.3* | *1.3* | *0.5* |
| L0-6 2–3 m—Sieve | 58.0 | 84.8 | 100.0 |
| L0-6 2–3 m—LD-PSA | 62.6 | 90.0 | 99.6 |
| *Difference* | *4.6* | *5.2* | *0.4* |
| L0-6 3–4 m—Sieve | 60.9 | 84.5 | 100.0 |
| L0-6 3–4 m—LD-PSA | 63.8 | 90.9 | 99.7 |
| *Difference* | *2.9* | *6.3* | *0.3* |
| L0-6 4–5 m—Sieve | 63.9 | 90.5 | 100.0 |
| L0-6 4–5 m—LD-PSA | 61.2 | 92.4 | 99.9 |
| *Difference* | *2.7* | *1.8* | *0.1* |
| L0-6 5–6 & 7–8 m—Sieve | 49.3 | 88.9 | 100.0 |
| L0-6 5–6 & 7–8 m—LD-PSA | 53.9 | 88.1 | 99.5 |
| *Difference* | *4.6* | *0.8* | *0.5* |
| L0-6 6–7 m—Sieve | 63.2 | 95.6 | 100.0 |
| L0-6 6–7 m—LD-PSA | 67.7 | 94.1 | 100.0 |
| *Difference* | *4.5* | *1.5* | *0.0* |
| L0-7 0–2 m—Sieve | 61.5 | 80.2 | 100.0 |
| L0-7 0–2 m—LD-PSA | 70.6 | 91.4 | 99.8 |
| *Difference* | *9.1* | *11.2* | *0.2* |
| L0-7 2–3 m—Sieve | 83.7 | 94.2 | 100.0 |
| L0-7 2–3 m—LD-PSA | 79.2 | 96.8 | 99.9 |
| *Difference* | *4.4* | *2.7* | *0.1* |
| L0-7 3–4 m—Sieve | 63.4 | 88.9 | 100.0 |
| L0-7 3–4 m—LD-PSA | 65.2 | 94.3 | 99.9 |
| *Difference* | *1.7* | *5.4* | *0.1* |
| L0-7 4–5 m—Sieve | 47.8 | 83.5 | 100.0 |
| L0-7 4–5 m—LD-PSA | 52.4 | 88.2 | 99.6 |
| *Difference* | *4.6* | *4.7* | *0.4* |
| L0-7 5–6 m—Sieve | 48.7 | 81.7 | 100.0 |
| L0-7 5–6 m—LD-PSA | 65.8 | 92.7 | 99.8 |
| *Difference* | *17.2* | *11.1* | *0.2* |
| L0-7 6–7 m—Sieve | 52.6 | 78.6 | 100.0 |
| L0-7 6–7 m—LD-PSA | 60.7 | 90.0 | 99.7 |
| *Difference* | *8.1* | *11.4* | *0.3* |
| L0-7 7–8 m—Sieve | 56.3 | 78.8 | 100.0 |
| L0-7 7–8 m—LD-PSA | 65.5 | 92.1 | 99.9 |
| *Difference* | *9.2* | *13.4* | *0.1* |
| L0-7 8–9 m—Sieve | 55.7 | 78.1 | 100.0 |
| L0-7 8–9 m—LD-PSA | 69.3 | 93.0 | 99.9 |

| Sample ID | <0.5 mm | 0.5–1 mm | 1–2 mm |
|---|---|---|---|
| *Difference* | *13.6* | *14.8* | *0.1* |
| LO-7 9–10 m—Sieve | 54.0 | 73.7 | 100.0 |
| LO-7 9–10 m—LD-PSA | 63.1 | 93.0 | 99.9 |
| *Difference* | *9.1* | *19.3* | *0.1* |
| Maximum Difference Cumulative % | 17.4 | 21.9 | 3.4 |
| Minimum Difference Cumulative % | 0.1 | 0.4 | 0.0 |
| Mean Difference Cumulative % | 7.7 | 7.8 | 0.4 |
| Median Difference Cumulative % | 7.2 | 5.3 | 0.2 |

# REPORT DOCUMENTATION PAGE

*Form Approved*
*OMB No. 0704-0188*

Public reporting burden for this collection of information is estimated to average 1 hour per response, including the time for reviewing instructions, searching existing data sources, gathering and maintaining the data needed, and completing and reviewing this collection of information. Send comments regarding this burden estimate or any other aspect of this collection of information, including suggestions for reducing this burden to Department of Defense, Washington Headquarters Services, Directorate for Information Operations and Reports (0704-0188), 1215 Jefferson Davis Highway, Suite 1204, Arlington, VA 22202-4302. Respondents should be aware that notwithstanding any other provision of law, no person shall be subject to any penalty for failing to comply with a collection of information if it does not display a currently valid OMB control number. **PLEASE DO NOT RETURN YOUR FORM TO THE ABOVE ADDRESS.**

| 1. REPORT DATE *(DD-MM-YYYY)* | 2. REPORT TYPE | 3. DATES COVERED *(From - To)* |
|---|---|---|
| February 2020 | Technical Report/Final | |

**4. TITLE AND SUBTITLE**

Sieve Stack and Laser Diffraction Particle Size Analysis of IMX-104 Low-Order Detonation Particles

**5a. CONTRACT NUMBER**

**5b. GRANT NUMBER**

**5c. PROGRAM ELEMENT NUMBER**

**6. AUTHOR(S)**

Matthew F. Bigl, Samuel A. Beal, Michael R. Walsh, Charles A. Ramsey, and Katrina M. Burch

**5d. PROJECT NUMBER**

**5e. TASK NUMBER**

**5f. WORK UNIT NUMBER**

**7. PERFORMING ORGANIZATION NAME(S) AND ADDRESS(ES)**

U.S. Army Engineer Research and Development Center (ERDC)
Cold Regions Research and Engineering Laboratory (CRREL)
72 Lyme Road
Hanover, NH 03755-1290

Envirostat, Inc.
PO Box 339
Vail, AZ 85641

**8. PERFORMING ORGANIZATION REPORT NUMBER**

ERDC/CRREL TR-20-3

**9. SPONSORING / MONITORING AGENCY NAME(S) AND ADDRESS(ES)**

Environmental Security Technology Certification Program
Environmental Restoration Program Area
4800 Mark Center Drive, Suite 16F16
Alexandria, VA 22350-3605

**10. SPONSOR/MONITOR'S ACRONYM(S)**

ESTCP

**11. SPONSOR/MONITOR'S REPORT NUMBER(S)**

**12. DISTRIBUTION / AVAILABILITY STATEMENT**

Approved for public release; distribution is unlimited.

**13. SUPPLEMENTARY NOTES**

Environmental Security Technology Certification Program (ESTCP) Environmental Restoration Program.
Funded by MIPR W74RDV80715663 and W74RDV90156248

**14. ABSTRACT**

When an artillery round undergoes a low-order detonation during live-fire training or an unexploded ordnance clearance operation, up to 25% of the round's energetic contents are scattered over a small, localized area, sometimes less than 100 $m^2$. Training-range fate and transport models require an accurate representation of the particle-size characteristics of the material left behind from low-order detonations.

This study investigated using laser diffraction particle size analysis to characterize 26 samples collected from four low-order command-detonated 81 mm mortar bodies filled with IMX-104. The refractive index of IMX-104 was estimated using an iterative recalculation technique on a Horiba LA-960 that yielded 1.845 0.01*i*. Of the 25 triplicate analyses conducted using this value, 12 passed the USP <429> measurement standard with 9 of the remaining samples found to have had a reduction in particle size during analysis that caused artificially high coefficient of variance values. The cumulative percent of particle sizes determined by laser diffraction and sieve stack differed by 0%–21.9% (median = 0.2%–7.2%). In addition, the higher resolution results of the laser diffraction particle size analysis, especially for particles smaller than 0.5 mm, make it the preferred method of analysis.

**15. SUBJECT TERMS**

Command detonation, Energetics, Explosives--Environmental aspects, Fate and transport, Insensitive munitions, Laser diffraction, Propellants--Residues, Soil pollution

| 16. SECURITY CLASSIFICATION OF: | | | 17. LIMITATION OF ABSTRACT | 18. NUMBER OF PAGES | 19a. NAME OF RESPONSIBLE PERSON |
|---|---|---|---|---|---|
| a. REPORT | b. ABSTRACT | c. THIS PAGE | | | 19b. TELEPHONE NUMBER *(include area code)* |
| Unclassified | Unclassified | Unclassified | SAR | 63 | |